THE JOURNAL OF PHYSICAL CHEMISTRY C

Article

Cite This: J. Phys. Chem. C 2018, 122, 21770−21783

pubs.acs.org/JPCC

Cation-Dependent Electrochemistry of Polysulfides in Lithium and Magnesium Electrolyte Solutions

Georg Bieker,[†] Diddo Diddens,[‡] Martin Kolek,*[,†] Oleg Borodin,[§] Martin Winter,[†,‡] Peter Bieker,*[,†] and Kirsi Jalkanen[†,∥]

[†]MEET Battery Research Center, Institute of Physical Chemistry, University of Münster, Corrensstrasse 28/30, 48149 Münster, Germany

[‡]Helmholtz Institute Münster (HI MS), IEK-12, Forschungszentrum Jülich GmbH, Corrensstrasse 46, 48149 Münster, Germany

[§]Electrochemistry Branch, Sensor and Electron Devices Directorate, U.S. Army Research Laboratory, Adelphi, Maryland 20783, United States

Supporting Information

ABSTRACT: In Li/S and Mg/S batteries, the charge and discharge of the sulfur cathode proceeds through a cascade of bivalent S_x^{2-} and radical $S_y^{\bullet-}$ polysulfide intermediates. The presence of Li^+ or Mg^{2+} cations in the electrolyte determines the type of intermediates and the overpotentials of their formation in a different manner. Based on systematic cyclic voltammetry (CV) and UV/vis investigations, this work reveals how the mutual interplay of the different cations, the electrolyte solvent, and the polysulfide anions is reflected in the electrochemical behavior of "Li_2S_8"/LiTFSI and "MgS_8"/$MgTFSI_2$ solutions with dimethyl sulfoxide, dimethylformamide, acetonitrile, dimethoxyethane, tetraethylene glycol dimethyl ether, or tetrahydrofuran as solvent. It was observed that the disproportionation reactions of the polysulfides are generally more pronounced and especially the $S_3^{\bullet-}$ radical is less stabilized in Mg^{2+} than in Li^+ containing solutions. In contrast to their Li counterparts, the formation of S_4^{2-} polysulfides during the reduction of sulfur is not observed in glyme-based Mg polysulfide solutions. Quantum chemical predictions of stability and disproportionation of the Mg/polysulfide/solvent clusters complemented the CV and UV/vis investigations.

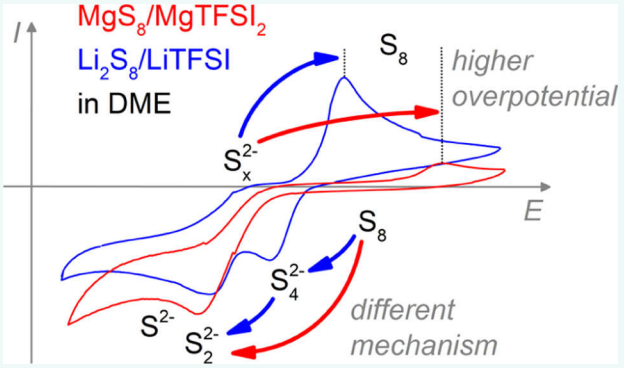

INTRODUCTION

Lithium/sulfur (Li/S) batteries are one of the most investigated high-energy battery systems, because the high theoretical specific capacity of the sulfur conversion cathode (1675 mA h/g) drastically outranges any Li^+ insertion cathode material[1] and the lithium metal anode possesses a very low electrochemical potential (−3.04 V vs SHE) and a high specific capacity (3862 mA h/g).[2] In contrast to most other cathode materials, sulfur is extremely cheap, highly abundant and comparably eco-friendly.[3,4] On the other hand, Li/S batteries use Li metal for the anode that depending on purity and shape, such as foil thickness can be a significant cost factor.[5] Furthermore, the low redox potential of Li metal comes with a high reactivity towards the electrolyte. Although it is slowed down by a solid electrolyte interphase, electrolyte decomposition and correlated corrosion of the anode are fundamental and yet unsolved challenges of Li/S batteries.[4,6−10] In addition, the heterogeneous dissolution and deposition of Li leads to the formation of high surface area lithium (HSAL),[9,11] which intensifies its corrosion. Furthermore, needle-like Li dendrites may cause a short-circuit of the cell, if they reach the cathode.[6,8,9,12−15] As also the abundance of Li is limited (only 18 mg/kg of the continental crust[16] and ≈0.2 mg/L in sea water[17,18]) and the price is comparably high,[5,19] it is attractive to develop metal/sulfur batteries with anodes that are safer, cheaper and more abundant than Li.

Other alkali metal anodes, like Na and K, have lower specific capacities and are even more reactive towards the electrolyte than Li. In contrast, multivalent Mg, Ca, and Al metal anodes possess high theoretical specific capacities (Mg: 2205 mA h/g, 3833 mA h/cm^3; Ca: 1340 mA h/g, 2077 mA h/cm^3; Al: 2980 mA h/g, 8046 mA h/cm^3) and a lower reactivity towards the electrolyte. Whereas rechargeable Al/S batteries have been demonstrated recently,[20,21] the development of Ca-metal based batteries still struggles with the insufficient Ca^{2+} conductivity in most of the Ca anode passivation layers.[22,23]

Received: July 9, 2018
Revised: August 27, 2018
Published: September 4, 2018

DOI: 10.1021/acs.jpcc.8b06560
J. Phys. Chem. C 2018, 122, 21770−21783

In case of Mg-based batteries, various electrolyte systems that avoid the formation of such a passivating layer on the anode while being also stable with the sulfur cathode could be developed.[24−30] Some of these allow the operation of Mg/S cells for hundreds of cycles.[24−36] In contrast to Li metal, Mg can be deposited and dissolved with a Coulombic efficiency of close to 100%[37−39] and the tendency to form dendrites is much lower. At the cathode, similar to Li/S batteries, sulfur is reduced to magnesium sulfide (MgS) and re-oxidized to sulfur:

$$\text{Anode: } Mg^0 \leftrightarrow Mg^{2+} + 2e^- \quad (1)$$

$$\text{Cathode: } S_8 + 8Mg^{2+} + 16e^- \leftrightarrow MgS \quad (2)$$

Assuming 1672 mA h/g cathode capacity and a mean discharge voltage of 1.77 V (vs 2.28 V for Li/S),[40] these reactions deliver high theoretical energy values of 1684 W h/kg and 3221 W h/L (vs 2654 W h/kg, 2856 W h/L for Li/S). As Mg is cheap[41] and highly abundant (22 g/kg of the continental crust[16] and ≈1 g/L in sea water[42]), its combination with a sulfur cathode could thus path the way to safer, more sustainable and potentially also more economic high-energy batteries.

Similar to Li/S cells, the reduction of sulfur at the cathode proceeds through dissolved Mg polysulfide MgS_x (x = 4−8) intermediates until insoluble MgS_2 is formed and is further reduced to MgS. In this complex solid−liquid−solid mechanism, practical Mg/S cells show lower capacities than the theoretical value. As for the Li/S system, this difference is commonly explained by the low accessibility of sulfur in the C/S composite cathode and by an incomplete discharge reaction (e.g., mixtures of MgS, MgS_2 and MgS_x polysulfides as final products)[24,26,29,31,32,35,36] due to an insufficient Mg polysulfide solubility and kinetic limitations of the solid phase magnesiation of MgS_2. The additional capacity fading is usually related (i) to the dissolution of sulfur[26,29,32] and Mg polysulfides[24−29,31,32,36] into the electrolyte (despite their low solubility[29,36,43]), (ii) to the resulting polysulfide-shuttle,[24,27−29,31,32] and especially (iii) to the irreversibility of the MgS/MgS_2 phase transition.[26,31,36] Consequently, limiting the discharge to the formation of MgS_2 largely improves the cycle life of Mg/S batteries.[36]

In addition, the overvoltages in Mg/S cells tend to be huge. Most publications show mean discharge voltages between 1.1 and 1.3 V or lower, whereas the typical mean charge voltages are at ≈2.0 V or higher.[24−27,29,31−35] This voltage gap results in poor energy efficiencies of current Mg/S cells. Whereas the overvoltages during charge and discharge are usually attributed to the overpotential of Mg deposition and dissolution at the anode,[27,29,35,36] also the processes at the S cathode should be regarded: in three-electrode cells, the mean discharge potential of the S cathode (1.4−1.5 V vs Mg/Mg^{2+})[29,36] differs significantly from the theoretical potential (1.77 V vs Mg/Mg^{2+}).[40] The overpotentials at the cathode are assigned to low electronic contact and/or insufficient pore volume inside the C/S composite[34−36] and to slow kinetics of the transformation of amorphous MgS_2 to crystalline MgS during discharge.[26,31,36]

Despite their central role during discharge and charge of Mg/S cells, the reduction and oxidation mechanism of Mg polysulfides has not been systematically investigated, yet. Concerning the discharge mechanism of Mg/S batteries several discrepancies exist in literature.[26,32,35,36] In total, four stages are proposed:[32]

$$\text{Stage 1: } S_8 + Mg^{2+} + 2e^- \rightarrow MgS_8 \quad (3)$$

$$\text{Stage 2: } MgS_8 + Mg^{2+} + 2e^- \rightarrow 2MgS_4 \quad (4)$$

$$\text{Stage 3: } MgS_4 + Mg^{2+} + 2e^- \rightarrow 2MgS_2 \quad (5)$$

$$\text{Stage 4: } MgS_2 + Mg^{2+} + 2e^- \rightarrow 2MgS \quad (6)$$

In the discharge of Mg/S cells with $Mg(HMDS)_2/AlCl_3/MgCl_2$ (HMDS = hexamethyldisilazide)-based electrolytes two voltage plateaus are observed.[28,31,34] According to their capacities, Zhao-Karger et al. assigned them to the direct reduction of S_8 to S_4^{2-} (stage 1 + 2) and its further reduction to S_2^{2-} (stage 3).[26]

However, in $MgTFSI_2/MgCl_2$ [TFSI = bis-(trifluoromethanesulfonyl)imide] in tetraethylene glycol dimethyl ether (TEGDME)/DOL (DOL = 1,3-dioxolane) electrolyte, Robba et al. also observed two voltage plateaus, but assigned them to the reduction of S_8 (stage 1) and the formation of MgS_2 (stage 2 + 3).[35] In quasi-equilibrium galvanostatic intermittent titration technique measurements with $MgTFSI_2$ in dimethoxyethane (DME) electrolyte, also Gao et al. distinguished between the initial voltage decrease (stage 1) and a large voltage plateau (stage 2 + 3).[36] However, for higher S/C ratios, only one voltage plateau (stage 1−3) is observed. For electrolytes of $Mg(BOR(hfip)_4)_2$ ($BOR(hfip)_4$ = tetrakis(hexafluoroisopropyloxy)borate) in glymes, only one voltage plateau is reported.[28,33]

In all Mg/S studies, the voltage plateaus (stage 1−3) are followed by a steep slope of the voltage until the cut-off voltage is reached.[24−29,31−36] This final step of the discharge is assigned to the slow solid phase transformation of previously precipitated MgS_2 to MgS (stage 4). In general, distinct potential plateaus in the discharge profiles usually disappear after several cycles and at higher discharge rates.[29,31−33] As intermediates remain in the electrolyte and on the cathode, the reaction stages are difficult to distinguish.

As the overpotentials of Mg/S batteries substantially differ from Li/S batteries, we aim for a better understanding of the influence of the Li^+ and Mg^{2+} cations in polysulfide reduction and oxidation processes. In order to examine the mutual interplay of the cation and the solvent, this study compares the behavior of Mg and Li polysulfide solutions in a large variety of solvents. Concerning the mechanistic discrepancies in Mg/S literature, it is of special interest, in which solvents the formation of S_8^{2-} (stage 1) occurs. Similar to the behavior of Li polysulfides, our previous study[43] already revealed that also Mg polysulfides form a complex system of disproportionation and dissociation equilibria:

]

$$\text{Disportionation: } S_8^{2-} \leftrightarrow S_6^{2-} + 1/4S_8 \quad (7)$$

$$S_8^{2-} \leftrightarrow S_4^{2-} + 1/2S_8 \quad (8)$$

$$S_6^{2-} \leftrightarrow S_4^{2-} + 1/4S_8 \quad (9)$$

$$\text{Dissociation: } S_6^{2-} \leftrightarrow 2S_3^{\bullet -} \quad (10)$$

These equilibria were found to depend on the properties of the solvent. Chemically prepared "MgS_8" and "Li_2S_8" disproportionates to S_6^{2-}, which partly dissociates to $S_3^{\bullet -}$ in high-ε solvents, like dimethyl sulfoxide (DMSO), dimethyl-

DOI: 10.1021/acs.jpcc.8b06560
J. Phys. Chem. C 2018, 122, 21770−21783

formamide (DMF), and acetonitrile (ACN). In contrast, in low-ε solvents, like DME, TEGDME, and tetrahydrofuran (THF), the equilibria are dominated by further disproportionation to S_4^{2-}.[43] According to these two characteristics, S_8^{2-}, S_6^{2-}, and $S_3^{\bullet-}$ are grouped as "low charge density" polysulfides in this study. Differing from the commonly used term "long-chain" polysulfides, this group includes the short $S_3^{\bullet-}$ radical. S_4^{2-} would thus refer to a "high charge density" polysulfide species.

As the Mg polysulfide equilibria and the UV/vis absorbance differ from the ones of Li polysulfides, differences in the cation-coordination of the polysulfides were deduced.[43] In order to investigate how these are reflected in the electrochemical behavior of the polysulfides, solutions of "Li_2S_8" and "MgS_8" in DMSO, DMF, ACN, DME, TEGDME, and THF were investigated via cyclic voltammetry (CV). As TFSI-based electrolytes are standard for Li/S[3,4] and increasingly investigated in Mg/S batteries,[25,29,35,36] LiTFSI and $MgTFSI_2$, respectively, were added as conducting salts.

In order to gain a deeper understanding of the stabilities of Mg polysulfides in comparison with Li polysulfides, quantum chemical calculations of the contact ion pair formation energies and the disproportionation equilibria of the Li and Mg polysulfide species in DMSO, DME, and THF were conducted.

EXPERIMENTAL SECTION

Preparation of "MgS_8"/$MgTFSI_2$ and "Li_2S_8"/LiTFSI Solutions. The preparation and electrochemical investigation of all polysulfide solutions were conducted in an argon-filled glove box (UNIlab by MBRAUN). Most solvents were used as received (ACN, 99.8%, Sigma-Aldrich; DME, 99.5%, Sigma-Aldrich; TEGDME, 99%, Sigma-Aldrich; *N*-methylimidazole (*N*-MeIm), 99%, Alfa Aesar; DMSO, 99.9%, Sigma-Aldrich; DMF, 99.8%, Sigma-Aldrich). THF (99.99%, Fisher Scientific) was dried in a solvent purification system over Al_2O_3 and degassed with argon inert gas. The "MgS_8" and "Li_2S_8" solutions were prepared as described in an earlier study.[43,44] Briefly, the "MgS_8" solutions were prepared by stirring $[Mg(N\text{-MeIm})_6]S_8$ (1 mM) in the investigated solvents. $[Mg(N\text{-MeIm})_6]S_8$ was synthesized from Mg powder (99.8%, Alfa Aesar) and sulfur (99.98%, Sigma-Aldrich) in *N*-MeIm (60 mL, 99%, Alfa Aesar). The "Li_2S_8" solutions were prepared from stoichiometric amounts of Li_2S (99.98%, Sigma-Aldrich) and sulfur (99.98%, Sigma-Aldrich) in the investigated solvent. "Li_2S_8" stock solutions (10 mM) were then diluted to 1 mM solutions. $MgTFSI_2$ (99.5%, Solvionic) was dried at 120 °C and 10^{-7} mbar for 72 h. LiTFSI (99.9%, <20 ppm H_2O, Solvionic) was used as received. $MgTFSI_2$ (0.05 M) and LiTFSI (0.10 M) were dissolved in the "MgS_8" (1 mM) and "Li_2S_8" (1 mM) solutions, respectively.

UV/Vis Measurements. In parallel to the electrochemical investigation of the "MgS_8"/$MgTFSI_2$ and "Li_2S_8"/LiTFSI solutions, the influence of the additional $MgTFSI_2$ and LiTFSI, respectively, on the polysulfide species was investigated in UV/vis spectroscopy. As described more in detail in our previous study,[43] the UV/vis measurements were conducted in a 2-channel spectrometer UV-2450 (Shimadzu) using sealed quartz glass cuvettes (Hellma Analytics, QS115) with a path length of 10 mm. Therefore, each sample solution was measured against the pure solvent reference spectrum.

CV Measurements. The CV experiments were carried out in flooded cells with two in PEEK embedded glassy carbon (GC) electrodes [working electrode (WE) and counter electrode (CE), 0.5 mm diameter] and an Ag/Ag^+ reference electrode (RE). A scheme of the electrochemical cell is depicted in Figure S8. The RE was composed of an Ag wire dipped in $AgNO_3$ (0.01 M, 99.5% Grüssing) in ACN solution, separated from the test solution by a polytetrafluoroethylene tube with a porous Vycor plug (eDAQ). It was washed with ethanol and ACN, dried and refilled with $AgNO_3$ in ACN solution before each measurement. After filling the cell with test solution (2 mL), the OCV was observed until a constant potential was reached (at least for 30 min). The CV of the "Li_2S_8"/LiTFSI or "MgS_8"/$MgTFSI_2$ sample solutions were recorded at 50 mV/s. Afterwards, ferrocene (5 mM, 0.01 mmol, 1.9 mg, 98%, Merck) was added to the sample solution and the oxidation and reduction potentials of the Fc/Fc^+ couple were detected against Ag/Ag^+ RE. The mean potential of the oxidation and the reduction peak was used to calibrate the previously detected voltammograms of the polysulfide solutions against ferrocene (Figure S9).

Computational Details. In addition to the experimental analyses, quantum chemical (QC) calculations have been performed to rationalize the solvation behavior and the trends observed in the UV/vis spectra of the individual cation/polysulfide species in the different solvents. Here, we focus on DME, DMSO, and THF to include representatives of solvents with low and high relative dielectric permittivities from the experimental part, as well as to compare chelating and non-chelating solvents.

All calculations have been performed with the Gaussian 09 package.[45] In particular, we performed two types of calculations: in the first step, we compared cation−polysulfide and cation−solvent dimers for various density functional theory (DFT) functionals and wave-function-based methods (see Table S1). As reported previously,[46,47] we found that the results obtained by the computationally expedient PBE functional[48] with a 6-31+G(d,p) basis show good agreement with the values from highly accurate but computationally expensive G4MP2 calculations.[49] In particular, the deviation between both methods is below 0.4 kcal/mol for the Li^+-solvent dimer binding energy, while it is somewhat larger for the Mg^{2+}-solvent dimers (roughly 2 kcal/mol). For dimers involving polysulfide anions, the deviations between PBE/6-31+G(d,p) and G4MP2 become larger with increasing polysulfide length (up to 13 kcal/mol for MgS_8), likely due to the fact that dispersion interactions are not fully captured by the DFT calculations. Including an empirical dispersion correction[50] in the DFT calculations partially mitigates these inaccuracies and reduces maximum deviations to 4 and 7 kcal/mol for Li_2S_8 and MgS_8, respectively. Unfortunately, addition of empirical dispersion in DFT PBE calculations results in larger deviations from the benchmark G4MP2 results for the cation−solvent dimer binding energies. Other DFT functional such as B3LYP or the use of different basis sets also yield slightly better agreement with G4MP2 for the cation−polysulfide interactions, whereas the prediction of the cation−solvent interactions becomes worse. Therefore, we use a correction obtained from dimer calculations to account for the deviations between PBE/6-31+G(d,p) and G4MP2 in the following (see below). An estimation of the counterpoise correction[51] revealed that the basis set superposition error is roughly 1 kcal/mol (corresponding to a relative error on the order of one percent), and was hence neglected.

DOI: 10.1021/acs.jpcc.8b06560
J. Phys. Chem. C 2018, 122, 21770−21783

Motivated by the good agreement between PBE/6-31+G(d,p) and G4MP2, we performed calculations of larger clusters resembling the real solvation shell in the electrolytes at the PBE/6-31+G(d,p) level in a second step. In our approach, the first solvation shell was modelled explicitly by an appropriate number of coordinating solvent molecules (in addition to the anions). Beyond the first coordination sphere, we employ an implicit solvation model mimicking the remainder of the electrolyte. This so-called cluster−continuum approach (CCA) has recently been demonstrated to yield accurate estimates of contact ion pair formation energies.[46,47] For the implicit solvent, the SMD model[52] has been utilized. For DMSO and THF, the built-in parameters have been used, while for DME, the solvent parameters for the implicit solvation model have been approximated by those of diethyl ether.

In order to determine the appropriate number of solvent molecules for each cluster, we performed free energy calculations based on the vibrational frequencies for clusters containing different numbers of solvent molecules within the SMD model. The resulting clusters with the lowest free energy are shown in Figures S11−S14. Overall, the coordination shells of the magnesium complexes tend to contain a larger number of coordinating molecules. To account for the deviations between PBE/6-31+G(d,p) and G4MP2 for the cation−anion interactions (see above), we calculated the energy/free energy difference between both methods for dimers in the implicit solvent (as opposed to the values in Table S1, which were calculated in vacuo), and used these differences as correction for the contact ion pair-formation energies and free energies. Typically, these corrections were in the range of 1−5 kcal/mol.

Based on the CCA, we estimated the contact ion pair formation energies relative to the fully solvated cations. In particular, we compared ion pairs consisting of the cations Li^+/Mg^{2+} and the bivalent polysulfide species S_2^{2-}, S_4^{2-}, S_6^{2-}, S_8^{2-}, the radical anion $S_3^{\bullet-}$, as well as $TFSI^-$, for the solvents mentioned above.

RESULTS AND DISCUSSION

DMSO, DMF, ACN. Due to their strong Mg salt dissociation power, the high-ε solvents DMSO,[53−56] DMF,[57,58] and ACN,[59−61] are frequently investigated as electrolyte solvents for Mg-based battery systems. In addition, DMSO[62−66] and DMF[66−69] are extensively studied in sulfur electrochemistry. As the reduction and oxidation mechanism of Li polysulfides in these high-ε solvents differs significantly from their behavior in low-ε ethers,[62,63] they are an attractive reference system to study the influence of the solvent also in Mg polysulfide solutions.

However, as DMSO,[70] DMF,[71] and ACN[59] are not stable against the Mg anode they are impractical for Mg/S electrolytes. Nevertheless, an artificial interphase formed on Mg could potentially enable the usage of these solvents.[72]

DMSO. "Li_2S_8" and "MgS_8" solutions were prepared by mixing stoichiometric amounts of Li_2S and S_8 or dissolving $[Mg(N\text{-}MeIm)_6]S_8$, respectively, in the investigated solvents (see Experimental Section). Afterwards, the corresponding $LiTFSI/MgTFSI_2$ salt was added. In order to produce comparable results, the concentration of the monovalent Li^+ was generally set twice as high as of the bivalent Mg^{2+}, whereas the concentration of "S_8^{2-}" polysulfides and $TFSI^-$ anions was kept constant.

Figure 1a shows the UV/vis spectra of "Li_2S_8"/LiTFSI (1 mM/0.1 M) and "MgS_8"/$MgTFSI_2$ (1 mM/0.05 M) in

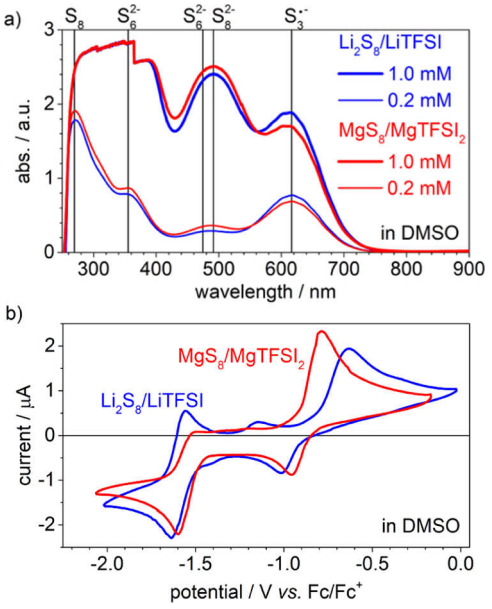

Figure 1. (a) UV/vis spectra of "Li_2S_8"/LiTFSI (1 mM/0.1 M) and "MgS_8"/$MgTFSI_2$ (1 mM/0.05 M) in DMSO solutions, and their 1:5 dilutions. (b) CVs of a GC electrode in these solutions at 50 mV/s, calibrated vs Fc/Fc^+.

DMSO solutions and their 1:5 dilutions. According to literature, the occurring absorbance peaks are assigned to S_8^{2-}, and to its disproportionation product S_6^{2-}, which further dissociates to $S_3^{\bullet-}$.[43] As the disproportionation of "Li_2S_8" and "MgS_8" in DMSO is limited to the formation of $S_6^{2-}/S_3^{\bullet-}$ and the UV/vis spectra of the Li/Mg polysulfide solutions are similar, an almost negligible influence of the Li^+ and Mg^{2+} cation on the polysulfides is deduced. This might be explained by the strong dielectric shielding of the cations by DMSO, which limits the interaction between Li^+/Mg^{2+} and the polysulfide anions.[43] The poor attraction is reflected in the comparatively low contact ion pair formation energies for the Li_2S_x and MgS_x species in DMSO (see Figure 9 in the Quantum Chemical Calculations section). In case of Mg^{2+}, the dissociation of S_6^{2-} to $S_3^{\bullet-}$ is less pronounced. A comparison of the "Li_2S_8"/"MgS_8" solutions with and without LiTFSI/$MgTFSI_2$ (Figure S1) indicates that higher Li^+/Mg^{2+} concentrations suppress the formation of $S_3^{\bullet-}$.

Figure 1b depicts the CVs of "Li_2S_8"/LiTFSI and "MgS_8"/$MgTFSI_2$ solutions. As the potential of Li metal is strongly influenced by the solvent of the sample solution[62] and we observed the same for Mg metal, the CV experiments were carried out with GC WE and CE, and a non-aqueous Ag/Ag^+ RE. In this setup, also the reactivity of the metals with the sample solutions can be excluded. However, the potential of the Ag/Ag^+ RE varies with the solvent of the sample solution.[62] In contrast, the redox potential of ferrocene (Fc/Fc^+) is considered to be relatively independent from the solvent.[73] Therefore, the voltammograms were calibrated versus the potential of the Fc/Fc^+ redox couple (see Experimental Section).

The CVs of the solutions of "Li_2S_8"/LiTFSI and "MgS_8"/$MgTFSI_2$ in DMSO show two main reduction processes starting at ≈−0.9 V and at −1.5 V (vs Fc/Fc^+). According to

DOI: 10.1021/acs.jpcc.8b06560
J. Phys. Chem. C 2018, 122, 21770−21783

the literature about Li polysulfides,[62−65] the first reduction wave refers to the reduction of S_8 to S_8^{2-} (stage 1). The formation of S_8^{2-} is accompanied by its disproportionation to S_6^{2-} and further dissociation to $S_3^{\bullet-}$.[63] These disproportionation and dissociation equilibria are confirmed in the UV/vis spectra of the "Li_2S_8" and "MgS_8" solutions (Figure 1a).[43] During further reduction of the Li polysulfides, a pre-wave at −1.4 V followed by a main reduction wave starting at −1.5 V (vs Fc/Fc^+) appears. In literature, the latter reduction wave is related to the formation of S_4^{2-}[62] or also S_3^{2-}.[63,64] The pre-wave at −1.4 V(vs Fc/Fc^+) is not observed in all studies.[62,66] It is either assigned to the direct formation of $S_3^{\bullet-}$[68] or the formation of S_4^{2-} and its disproportionation to $S_3^{\bullet-}$.[63] The Mg polysulfide solution shows a reduction process below −1.5 V (vs Fc/Fc^+), which is thus also referred to the formation of S_4^{2-} (stage 2) and/or S_3^{2-}.

During oxidation, the Li and Mg polysulfide solutions behave differently. In the CV of the Li polysulfide solution, three oxidation waves are observed. In some studies, the first and the second peak at −1.6 and −1.2 V are assigned to the formation of S_4^{2-}, $S_3^{\bullet-}$, and S_6^{2-} and their subsequent oxidation to S_8^{2-}.[63] In other studies, they are assigned to the oxidation of S_4^{2-} to S_8^{2-} and the oxidation of S_8^{4-} to S_8^{2-}.[62] However, the reduction of the low charge density ("long-chain") polysulfides S_8^{2-}, $S_6^{2-}/S_3^{\bullet-}$ to the high charge density ("short-chain") polysulfides S_4^{2-} and/or S_3^{2-} appears to be reversible in the presence of Li^+ cations.

In the Mg polysulfide solutions, only one oxidation step can be observed. The process above −1.0 V/−0.8 V (vs Fc/Fc^+) can be correlated to direct oxidation of all polysulfide species to sulfur.[62−64] The intermediate oxidation of high charge density (S_4^{2-}/S_3^{2-}) to low charge density polysulfides (S_8^{2-}, $S_6^{2-}/S_3^{\bullet-}$) is hardly observed.

DMF. The peaks of the UV/vis absorbance spectra of Li and Mg polysulfide solutions in DMF are assigned to S_8^{2-}, S_6^{2-}, and $S_3^{\bullet-}$ (Figure 2a).[43,68] In comparison with the solutions in DMSO, the dissociation of S_6^{2-} to $S_3^{\bullet-}$ is generally stronger in DMF, but also the restrictive effect of LiTFSI/$MgTFSI_2$ on this equilibrium is more pronounced (Figure S2). As in DMSO, the $S_3^{\bullet-}$ species are less stabilized if Mg^{2+} instead of Li^+ is the counter-cation.

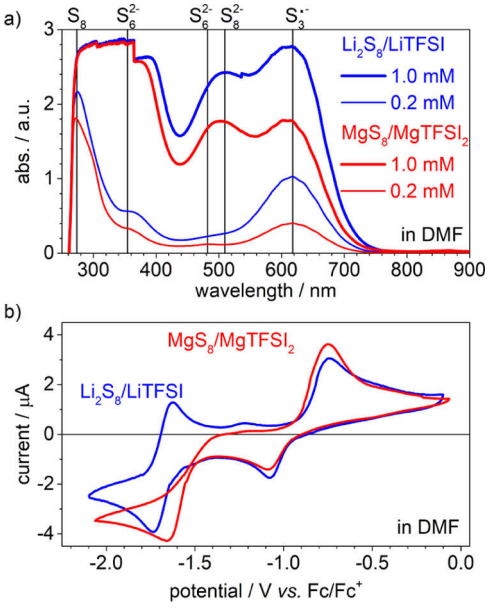

Figure 2. (a) UV/vis spectra of "Li_2S_8"/LiTFSI (1 mM/0.1 M) and "MgS_8"/$MgTFSI_2$ (1 mM/0.05 M) in DMF solutions, and their 1:5 dilutions. (b) CVs of a GC electrode in these solutions at 50 mV/s, calibrated vs Fc/Fc^+.

The similarities to the DMSO solutions are also reflected in the electrochemical behavior (Figure 2b). Also in DMF, the voltammograms of the Li and Mg polysulfide solutions show a first reduction wave below −1.0 V (vs Fc/Fc^+), which is related to the formation of S_8^{2-} and its disproportionation to $S_6^{2-}/S_3^{\bullet-}$ (compare Figure 2a).[67−69] A small pre-wave at −1.5 V (vs Fc/Fc^+), which Gaillard and Levillain assigned to the electrochemical formation of $S_3^{\bullet-}$,[68] is again only visible in the Li polysulfide solution. It is followed by a reduction process that is generally assigned to the formation of S_4^{2-}[69] or also S_3^{2-}.[67] In the Mg polysulfide solution, this reduction wave already starts at ≈−1.5 V (vs Fc/Fc^+). During oxidation of the Li polysulfide solution, peaks at −1.7 and −1.2 V (vs Fc/Fc^+) occur. According to literature, these correlate with an increase of $S_3^{\bullet-}$ and S_8^{2-}, respectively.[68] The previous reduction of these species to S_4^{2-}/S_3^{2-} thus appears to be reversible. In the Mg polysulfide in DMF solution the first oxidation step, which is referred to the formation of $S_3^{\bullet-}$ from S_4^{2-}/S_3^{2-}, is not detected at all. Nevertheless, the formation of S_8^{2-} is indicated by a small oxidation wave at −1.2 V (vs Fc/Fc^+). Above −0.9 V (vs Fc/Fc^+) the formation of sulfur is observed in both, Li and Mg polysulfide solutions. As in DMSO, the higher currents occurring in the CV of the Mg polysulfide solution might indicate also the direct re-oxidation of high charge density polysulfides (S_4^{2-}/S_3^{2-}) to sulfur.

ACN. The electrochemical reduction of sulfur/polysulfide solutions in ACN is barely studied in literature.[66,74] Although its high relative dielectric permittivity (ε = 38.0) is comparable to DMSO (ε = 45.0) and DMF (ε = 36.1), the Gutmann donor number of ACN (DN = 14.1) is much lower than that of DMSO (DN = 29.8) or DMF (DN = 26.6).[75] Therefore, the Li and Mg polysulfide solutions in ACN show complex characteristics. On the one hand, the solubility of $[Mg(N\text{-}MeIm)_6]S_8$ in ACN is below 1 mM, which might be assigned to the low donor number.[43] On the other hand, "Li_2S_8" and "MgS_8" solutions in ACN show both disproportionation of S_8^{2-} to S_6^{2-} and further dissociation to $S_3^{\bullet-}$ (Figure S3).[74] This similarity to the solutions in DMSO and in DMF is related to the similar relative dielectric permittivity,[63] which might result in a more effective separation of Li^+/Mg^{2+} and the polysulfide anions and thus limits the influence of the cations towards further disproportionation.[43]

Interestingly, the addition of LiTFSI and $MgTFSI_2$ has a very different effect on the presence of polysulfide species. In the UV/vis spectra of the Li polysulfide solutions (Figure 3a), the absorption band of S_6^{2-} almost disappears and $S_3^{\bullet-}$ strongly decreases after addition of LiTFSI. Furthermore, the spectra of "Li_2S_8"/LiTFSI in ACN shows a shoulder at 425 nm, which is assigned to S_4^{2-}. With higher concentrations of Li^+, the disproportionation of "Li_2S_8" in ACN thus resembles the typical behavior in low-ε solvents such as DME, TEGDME, and THF (see below). This similarity continues in the electrochemical behavior of the Li polysulfide solutions (Figure 3b), which was also described by Jung et al.[66] In the cathodic scan, two reduction waves occur. The peak at −1.0 V (vs Fc/Fc^+) is referred to the formation of S_8^{2-} followed by disproportionation to $S_6^{2-}/S_3^{\bullet-}$, whereas the peak at −1.3 V (vs Fc/Fc^+) is assigned to the formation of

DOI: 10.1021/acs.jpcc.8b06560
J. Phys. Chem. C 2018, 122, 21770−21783

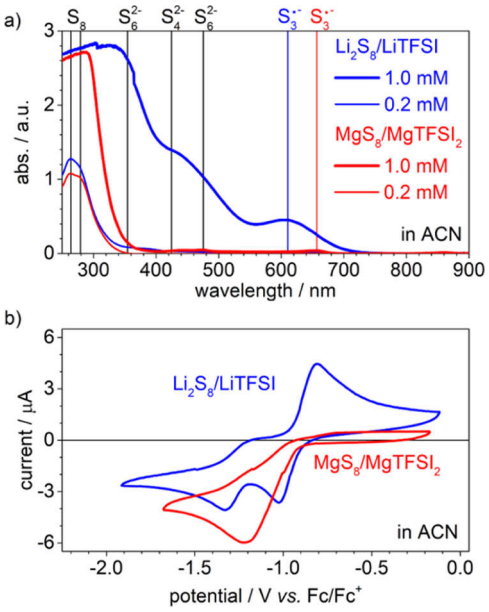

Figure 3. (a) UV/vis spectra of "Li_2S_8"/LiTFSI (1 mM/0.1 M) and "MgS_8"/$MgTFSI_2$ (1 mM/0.05 M) in ACN solutions, and their 1:5 dilutions. (b) CVs of a GC electrode in these solutions at 50 mV/s, calibrated vs Fc/Fc^+.

S_4^{2-}.[74] In ACN, the second reduction wave is thus observed at significantly higher potentials than in DMSO and DMF. During the anodic scan, the shoulder at −1.2 V (vs Fc/Fc^+) indicates the end of the second reduction process, but no reverse oxidation wave occurs. The formation of low charge density polysulfides ($S_6^{2-}/S_3^{\bullet-}$) through oxidation of high charge density polysulfides (S_4^{2-}) is thus not observed in ACN. In contrast, the broad oxidation process starting at −1.0 V (vs Fc/Fc^+) might include their direct oxidation to sulfur.

In the Mg polysulfide solutions, the addition of $MgTFSI_2$, surprisingly, leads to a higher solubility of $[Mg(N\text{-MeIm})_6]S_8$. Whereas its solubility in pure ACN is below 1 mM,[43] $[Mg(N\text{-MeIm})_6]S_8$ instantly dissolves at this concentration in $MgTFSI_2$ (0.05 M) in ACN solutions. However, UV/vis spectra of these "MgS_8"/$MgTFSI_2$ solutions (Figure 3a) indicate only very low concentrations of $S_6^{2-}/S_3^{\bullet-}$ and S_4^{2-}. It might be concluded that "MgS_8" does not only disproportionate to $S_6^{2-}/S_3^{\bullet-}$, as observed in the (supernatant) ACN solutions without $MgTFSI_2$ (Figure S3), but also forms disproportionation products, like S_2^{2-}, which are not detectable in UV/vis.

The voltammogram of "MgS_8"/$MgTFSI_2$ in ACN solution in Figure 3b shows only one reduction peak (−1.2 V vs Fc/Fc^+). This process already starts at −0.9 V versus Fc/Fc^+, and thus might include both, the formation of S_8^{2-}, $S_6^{2-}/S_3^{\bullet-}$ and the formation of S_4^{2-}. However, as S_8^{2-} and $S_6^{2-}/S_3^{\bullet-}$ are barely stabilized in the "MgS_8"/$MgTFSI_2$ in ACN solution (Figure 3a), the direct formation of S_4^{2-} and further reduced species are considered the main reduction process. In the anodic scan, the oxidation process at ≈−0.7 V (vs Fc/Fc^+), which is assigned to the oxidation of Mg polysulfide species to sulfur, shows low currents. As the UV/vis spectra reveal, these might refer to the low availability of polysulfides in the "MgS_8"/$MgTFSI_2$ in ACN solution (Figure 3a).

Ethers. As they are comparatively stable against the metal anodes, ethers are the typical electrolyte solvents for Li/S and Mg/S batteries. In Mg/S batteries, the electrolyte solvents are usually based on DME,[25,29,36] diglyme,[25,26,33,34] TEGDME,[26,31−33,35] or THF.[24,27] In Li/S batteries, solutions of LiTFSI in DOL/DME (1:1) are the standard electrolytes.[3,4] Therefore, we studied the electrochemical behavior of Li and Mg polysulfides in THF, DME, and TEGDME solutions.

In general, the solubility of $[Mg(N\text{-MeIm})_6]S_8$ in solutions of $MgTFSI_2$ (0.05 mM) in THF, DME, or TEGDME was determined to be between 10 and 100 mM. A similar solubility of Mg polysulfides have been described by others.[36] Interestingly, the solubility of $[Mg(N\text{-MeIm})_6]S_8$ in these ethers without addition of $MgTFSI_2$ is only between 1 and 10 mM.

DME and TEGDME. The UV/vis absorbance spectra of "Li_2S_8" in DME or TEGDME show the absorption bands of S_4^{2-} and $S_3^{\bullet-}$ (Figures S4 and S5). As S_8^{2-} is not stabilized, it disproportionates into sulfur and S_6^{2-}, which either dissociates to $S_3^{\bullet-}$ or further disproportionates to S_4^{2-}. Whereas a strong interaction of the Li^+ cation with the polysulfide species is assumed to induce further disproportionation to polysulfides with a higher charge density, like S_4^{2-}, a "shielding" of the cation by the solvent already stabilizes polysulfides with a lower charge density, like S_8^{2-}, S_6^{2-}, and $S_3^{\bullet-}$ (as in DMSO and DMF). In DME, the strong attraction of the polysulfides and Li^+ is reflected in high contact ion pair formation energies (see Figure 9 in the Quantum Chemical Calculations section). The relative dielectric permittivity and donor number of DME (ε = 7.2, DN = 18.6), TEGDME (ε = 7.7, DN = 16.6), and THF (ε = 7.6, DN = 20.0), are similar, but as the solutions of "Li_2S_8" in TEGDME shows higher concentrations of $S_3^{\bullet-}$, still a stronger coordination of Li^+ by TEGDME is deduced. This stabilization is assumed to be due to the effective "caging" of Li^+ through the chelate effect of TEGDME.[43] In DME and TEGDME, the addition of LiTFSI does not significantly affect the Li polysulfide species (Figures 4a and 5a).

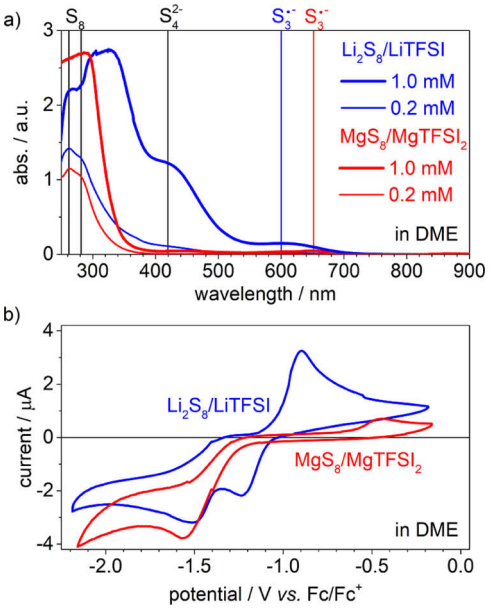

Figure 4. (a) UV/vis spectra of "Li_2S_8"/LiTFSI (1 mM/0.1 M) and "MgS_8"/$MgTFSI_2$ (1 mM/0.05 M) in DME solutions, and their 1:5 dilutions. (b) CVs of a GC electrode in these solutions at 50 mV/s, calibrated vs Fc/Fc^+.

DOI: 10.1021/acs.jpcc.8b06560
J. Phys. Chem. C 2018, 122, 21770−21783

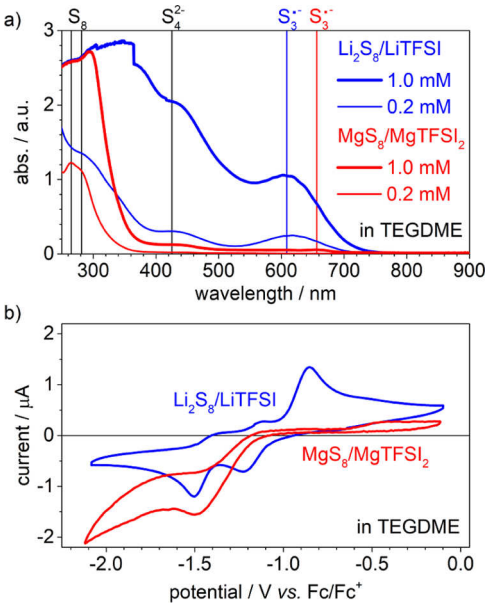

Figure 5. (a) UV/vis spectra of "Li_2S_8"/LiTFSI (1 mM/0.1 M) and "MgS_8"/$MgTFSI_2$ (1 mM/0.05 M) in TEGDME solutions, and their 1:5 dilutions. (b) CVs of a GC electrode in these solutions at 50 mV/s, calibrated vs Fc/Fc^+.

During reduction, both "Li_2S_8"/LiTFSI solutions show peaks at −1.2 and −1.5 V (vs Fc/Fc^+) (Figures 4b and 5b). For DME,[66] and DOL/DME (1:1),[62,63] similar profiles are observed in literature. According to Zou and Lu, the first reduction wave refers to the formation of S_4^{2-} and the second to further reduction to S_2^{2-} and S^{2-}.[63] In a different set-up, Barchasz et al. additionally observed the formation of S_8^{2-} and its further disproportionation to $S_6^{2-}/S_3^{\bullet-}$ at higher potentials (2.4 V vs Li/Li^+).[76] However, although the $S_3^{\bullet-}$ radical is observed in the UV/vis spectra of the Li polysulfide solutions in DME and TEGDME (Figures 4a and 5a), this process is not observed in our CV experiments. According to the observations in DMSO, DMF, and ACN (Figures 1b−3b), the formation of S_8^{2-} (and $S_6^{2-}/S_3^{\bullet-}$) would have been expected at ≈−1.0 V (vs Fc/Fc^+).

In the anodic scan of the Li polysulfide solutions in TEGDME, an oxidation process is detected at −1.1 V (vs Fc/Fc^+). As neither S_8^{2-} nor S_6^{2-} were found to be stable in "Li_2S_8" in TEGDME solutions (Figure 5a), this process indicates the formation of $S_3^{\bullet-}$. In DME, this oxidation process is not observed, which correlates with a lower presence of the radical in the "Li_2S_8" solutions (Figure 4a). However, the Li polysulfide solutions in DME and TEGDME both show the oxidation of all polysulfide species to sulfur above ≈−1.0 V (vs Fc/Fc^+).[63]

The Mg polysulfide solutions in DME and TEGDME differ strongly from their Li counterparts. Already in the UV/vis spectra of pure "MgS_8" in DME, S_4^{2-} and $S_3^{\bullet-}$ are hardly observed, and the addition of $MgTFSI_2$ even lowers their absorbance intensity (Figures 4a and S4). In TEGDME, both species are detected with slightly higher intensities (Figures 5a and S5). The disproportionation of the Mg polysulfides might proceed further to UV/vis insensitive species, like S_2^{2-}. In any case, the strong interaction between Mg^{2+} and the polysulfide anions can be deduced from the high contact ion pair formation energies (see Figure 9 in the Quantum Chemical Calculations section).

The lower stabilization of S_4^{2-} and $S_3^{\bullet-}$ strongly affects the electrochemical behavior of the Mg polysulfide solutions (Figures 4b and 5b). During reduction, only one peak is observed in the "MgS_8"/$MgTFSI_2$ in DME and TEGDME solutions. As neither $S_3^{\bullet-}$ nor S_4^{2-} show strong intensities in the UV/vis spectra of the "MgS_8" solutions, their formation is not expected during the cathodic scan. According to the potentials observed in the CVs of Li polysulfide solutions[63] the reduction peak at ≈−1.5 V (vs Fc/Fc^+) is referred to the direct transformation of sulfur to S_2^{2-}.[36] The electrochemical formation of the S_4^{2-} intermediate is thus not observed in Mg^{2+} containing solutions in DME and TEGDME. Figure S7 shows further reduction of the Li and Mg polysulfides in DME. In accordance with Gao et al. the peak at −2.4 V is consequently referred to the formation of S^{2-}.[36] As these species cannot be re-oxidized in our experimental setup, the reduction processes diminish during subsequent cycles.

In conclusion, the reduction pathway of sulfur in DME and TEGDME solutions depends on the presence of either Li^+ or Mg^{2+} cations. Whereas the reduction proceeds through the formation of the high charge density S_4^{2-} intermediate in case of Li, a direct conversion to S_2^{2-} is observed in case of Mg. In the following, the S_2^{2-} species are considered to be further reduced to S^{2-} in both kinds of solutions. The different mechanisms are illustrated in Figure 6.

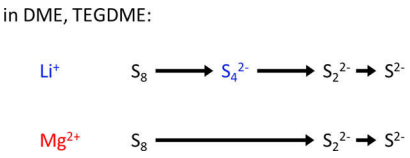

Figure 6. Scheme of the proposed sulfur reduction pathway in glymes. In the CV of Li polysulfide solutions the formation of the S_4^{2-} intermediate occurs, whereas only a direct transformation of S_8 to S_2^{2-} is observed in the Mg polysulfide solutions. The formation of low charge density polysulfides (S_8^{2-}, S_6^{2-}, $S_3^{\bullet-}$) is only observed in the CV of the Li and Mg polysulfide solutions in DMSO and DMF.

During oxidation of the Mg polysulfide solutions, the formation of sulfur occurs only above −0.5 V (vs Fc/Fc^+). In comparison with Li polysulfide in DME or TEGDME solutions (Figures 4b and 5b), the overpotential is referred to the coordination of the polysulfides by Mg^{2+}. It might be explained by the high contact ion pair formation energies/the stabilization of all MgS_x species observed in DFT calculations (see Figure 9).

The low currents detected during oxidation are referred to the low concentration of Mg polysulfides in the sample solutions (Figures 4a and 5a). Ongoing experiments with higher Mg polysulfide concentrations show higher intensities for the formation of sulfur.

THF. The UV/vis absorption spectra of the "Li_2S_8" and "MgS_8" solutions in THF only show low intensities for $S_3^{\bullet-}$ and the peaks for S_6^{2-} or S_8^{2-} are not visible (Figures 7a and S7). In the Li polysulfide solution, the shoulder at 425 nm indicates that S_8^{2-} disproportionates further than in the high-ε solvents and thus only S_4^{2-} is stabilized.[77] Although this shoulder is shifted to ≈380 nm in the Mg polysulfide solution, it was also assigned to S_4^{2-} in our previous work.[43] We concluded a strong electron withdrawing effect of the Mg^{2+} coordination on S_4^{2-}. However, although a low solubility of this species would be assumed, this shoulder might also refer

DOI: 10.1021/acs.jpcc.8b06560
J. Phys. Chem. C 2018, 122, 21770−21783

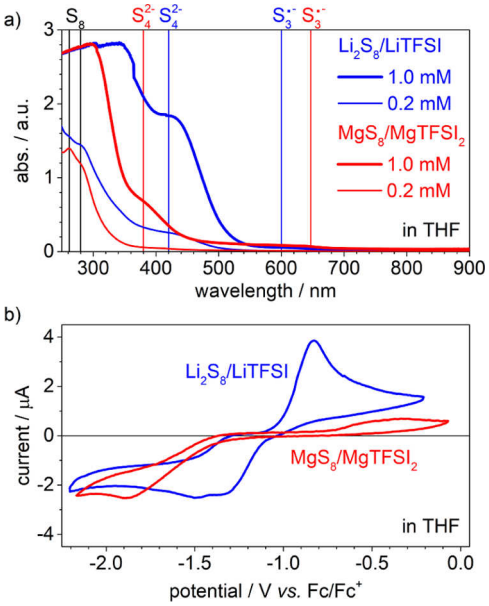

Figure 7. (a) UV/vis spectra of "Li_2S_8"/LiTFSI (1 mM/0.1 M) and "MgS_8"/$MgTFSI_2$ (1 mM/0.05 M) in THF solutions, and their 1:5 dilutions. (b) CVs of a GC electrode in these solutions at 50 mV/s, calibrated vs Fc/Fc^+.

to S_3^{2-}.[77] This would indicate that Mg^{2+}—unlike Li^+—coordination induces even further disproportionation of the polysulfides in THF. However, as the disproportionation of "Li_2S_8" and "MgS_8" proceeds to the high charge density S_4^{2-}/S_3^{2-} and the UV/vis spectra differ significantly between the Li^+ and Mg^{2+} containing solutions, a strong interaction between the cations and the polysulfide anions is deduced. Consequently, the high contact ion pair formation energies (Figure 9 in the Quantum Chemical Calculations section) indicate a strong attraction. Adding LiTFSI to "Li_2S_8" solution does not significantly affect the Li polysulfide species (Figure S7). In contrast, the addition of $MgTFSI_2$ to the "MgS_8" solutions decreases the intensity of S_4^{2-}/S_3^{2-}. As in DME and TEGDME they might further disproportionate into UV/vis insensitive and/or insoluble species, like S_2^{2-}.

The disproportionation of the "Li_2S_8" and "MgS_8" solutions in THF is reflected in the electrochemical behavior. As neither S_8^{2-} nor S_6^{2-}/$S_3^{\bullet-}$ are stabilized in the "Li_2S_8" and "MgS_8" solutions (Figure 7a), the peak at −1.0 V (vs Fc/Fc^+), which is assigned to the formation of S_8^{2-} and S_6^{2-}/$S_3^{\bullet-}$ in DMSO, DMF, and ACN, does not occur in THF (Figure 7b). In the Li polysulfide solutions a reduction wave with two peaks at −1.3 V and at −1.5 V (vs Fc/Fc^+) occurs. According to the potentials observed in DME and TEGDME, the first wave would be assigned to the formation of S_4^{2-} and the second to further reduction to S_2^{2-}. In the anodic scan, no corresponding (re-)oxidation process is observed until S_8 formation occurs (above −1.1 V vs Fc/Fc^+).

The reduction of the Mg polysulfides in THF only starts at ≈−1.3 V (vs Fc/Fc^+). However, the current of this process increases slowly and a maximum is only reached at ≈−1.9 V (vs Fc/Fc^+). As S_4^{2-} (or S_3^{2-}) has been observed to be a stable product of the disproportionation of "MgS_8" in THF (Figure 7a), it is expected that the electrochemical reduction of sulfur also proceeds through this species. However, according to the low potential of the correlated peak, this reduction process might rather correspond to the direct formation of S_2^{2-}. During oxidation, the formation of sulfur is only observed above −0.7 V (vs Fc/Fc^+). The oxidation of the polysulfides is thus also considered a slow reaction. According to the UV/vis spectra (Figure 7a), the low currents of this re-oxidation are assumed to reflect the low availability of Mg polysulfides in the sample solution. The huge hysteresis between the reduction and oxidation potential correlates with the observations made in DME and TEGDME (Figures 4b and 5b).

Quantum Chemical Calculations. In the UV/vis investigations, we found several differences between the disproportionation/dissociation equilibria in "Li_2S_8" and "MgS_8" solutions. In general, the disproportionation of S_8^{2-}, S_6^{2-}/$S_3^{\bullet-}$, and S_4^{2-} to sulfur and insoluble or UV/vis insensitive species was observed to be intensified by Mg^{2+} instead of Li^+ coordination. In order to provide a theoretical basis for these findings, and to unravel the impact of the cation species (i.e., Li^+, Mg^{2+}) on the polysulfide equilibria, we examined the stability of the lithium and magnesium solvates using quantum chemistry (QC) calculations. To this end, we computed the relative stability of larger cation/polysulfide/solvent clusters using a CCA, where the solvent in the first solvation shell is explicitly included in calculations, while the solvent in the second solvation shell and beyond is included via an implicit solvent model developed by the Minnesota group (SMD model). DFT calculations were performed using PBE functional and a compact 6-31+G(d,p) basis set. The Experimental Section provides computational details, while Table S1 compares the solvate binding energies from the computationally expedient DFT calculations with those obtained from more reliable but also much more computationally expensive composite methods such as G4 and G4MP2.[78] In particular, we calculated the contact ion pair-formation energies ΔE_{CIP} (i.e., at 0 K, including zero-point correction) and free energies ΔG_{CIP} (at 298 K) upon bringing a fully solvated cation and an anion from an infinite distance into contact via the CCA described above. For the sake of simplicity, we mainly restrict ourselves to the bivalent polysulfide species S_2^{2-}, S_4^{2-}, S_6^{2-}, and S_8^{2-}, and only consider complexes without a net charge.

Figure 8 shows four representative optimized complex structures for Li^+ and Mg^{2+} in combination with S_4^{2-} and S_6^{2-} surrounded by an explicit first coordination sphere consisting of DME molecules (in addition to the implicit solvent). The geometries of all clusters are shown in Figures S11−S14. Overall, the small cations are buried inside the cluster and avoid contact with the boundary region of the implicit solvent.

The results for the contact ion pair formation free energies ΔG_{CIP} are shown in Figure 9 as a function of the polysulfide chain length n (see also Table S2 for the detailed values of both ΔE_{CIP} and ΔG_{CIP}, and Table S5 for the formal reaction equations used to compute these energies). We note that all contact ion pair formation free energies are significantly negative, indicating pronounced ion pairing or clustering in the electrolyte solutions. In all cases, ΔG_{CIP} becomes more negative for shorter polysulfide chains, while the associated entropy change, reflected by the difference between ΔE_{CIP} and ΔG_{CIP}, is approximately constant (Table S2). Thus, the comparison between ΔE_{CIP} and ΔG_{CIP} reveals that the decrease of ΔG_{CIP} is mainly due to the increased charge density of the anion, which tends to maximize the energetic Coulomb attraction, as ΔE_{CIP} is mostly negative and displays similar trends as ΔG_{CIP}. The only exceptions, however, are the

DOI: 10.1021/acs.jpcc.8b06560
J. Phys. Chem. C 2018, 122, 21770−21783

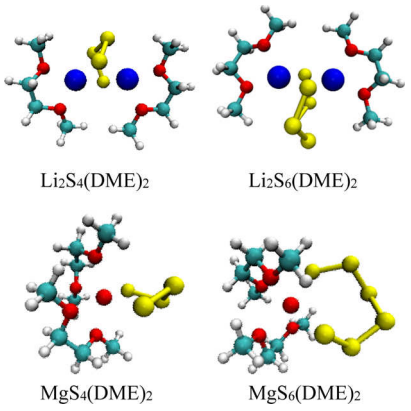

Figure 8. Optimized geometries of four representative contact ion pair clusters containing Li^+ and Mg^{2+} in combination with S_4^{2-} and S_6^{2-} in the solvent DME (modeled by both an explicit first coordination sphere and the implicit SMD solvation model for the remainder of the electrolyte). The calculations were performed at the PBE/6-31+G(d,p) level. Further cluster structures are shown in Figures S11–S14.

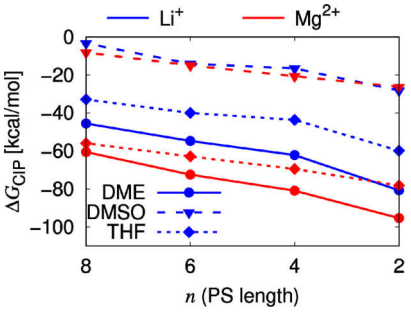

Figure 9. Contact ion pair formation free energies upon bringing a fully solvated Li^+/Mg^{2+} ion and a solvated polysulfide anion into contact as a function of the polysulfide chain length n (i.e., in terms of monomers) in different solvents. Blue curves show the free energies for Li^+, the red curves show the respective values for Mg^{2+}. The calculations were performed at the PBE/6-31+G(d,p) level of theory using the implicit SMD solvation model.

polysulfides larger than S_2^{2-} in DMSO, for which ΔE_{CIP} is positive. This is in line with the good solubility of "Li_2S_8" and "MgS_8" in DMSO, as well as with the larger relative dielectric permittivity and the large donor number of this solvent. Therefore, in this case, the formation of ion pairs or clusters apparently is entropically driven (see also below).

For DMSO and THF, the ΔG_{CIP} values (see Table S2), are significantly lower than the respective ΔE_{CIP} values, indicating that the release of solvent molecules from the solvation shell of the cations (at least two molecules, if the polysulfide anion coordinates in a bidentate fashion) leads to an entropy gain. In contrast, the entropic penalty arising from the complexation of the polysulfide chain seems to play a minor role, even though one would expect that especially for long-chain polysulfide species, the conformational phase space of the anion becomes somewhat reduced when engaged in an ion cluster. For the chelating solvent DME, we observe for both Li^+ and Mg^{2+} that ΔE_{CIP} and ΔG_{CIP} are basically identical, demonstrating that in this case entropic effects are negligible. This might be related to the fact that upon contact ion pair formation, a bidentate solvent molecule is exchanged by a bidentate polysulfide anion, which mainly constitutes a change in the internal energy, but is rather invariant for the entropic contribution.

When comparing Li^+ and Mg^{2+}, we note that in DMSO the contact ion pair formation energies and free energies are basically comparable, whereas ΔG_{CIP} is substantially smaller for the magnesium polysulfides in case of the ethers THF and DME (Figure 9). The behavior in the former solvent can again be rationalized by its good solvation properties, reflected by the solvent characteristics, that is the large relative dielectric permittivity and the high donor number of DMSO. In the ether-based electrolytes, electrostatic interactions are less screened by the solvent, resulting in lower contact ion pair formation energies for the "MgS_8" solutions as compared to the "Li_2S_8" solutions. Therefore, due to the bivalent charge of the cation, ion clustering is expected to be more pronounced for Mg^{2+} than for Li^+.

So far, we only considered the relative stability of the cation–polysulfide clusters, but not of the polysulfide species themselves, which may interconvert to each other by disproportionation reactions. To assess this effect, we additionally calculated the energies ΔE_D and free energies ΔG_D for the disproportionation reactions of the bare polysulfide anions, that is $S_8^{2-} \rightarrow S_6^{2-} + 1/4S_8$ and $S_8^{2-} \rightarrow S_4^{2-} + 1/2S_8$, and $S_8^{2-} \rightarrow S_2^{2-} + 3/4S_8$, in DMSO, DME, and THF at the G4MP2 level. Through the above formal reactions, the main polysulfide species S_6^{2-}, S_4^{2-}, and S_2^{2-} are directly linked to the initially present anion S_8^{2-}, thus allowing us to estimate their relative stability, although the detailed disproportionation mechanism may in principle be highly complicated. The results are shown in Figure 10 (see

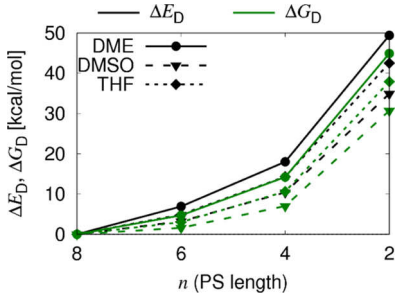

Figure 10. Disproportionation energies and free energies of the bare polysulfide anions in DMSO, THF, and DME (SMD solvation model) as a function of the polysulfide chain length n (in terms of monomers). The calculations have been performed at the G4MP2 level of theory.

Table S3 for the detailed values). Overall, the values are in qualitative agreement with previous QC calculations of polysulfide reactions[79] (albeit using different solvent parameters). We note that the free energies of the disproportionation reactions are significantly positive in all three solvents (at least 3 kcal/mol for the formation of S_6^{2-}, at least 10 kcal/mol for the formation of S_4^{2-}, far exceeded by at least 35 kcal/mol for the formation of S_2^{2-}). These observations can be rationalized by electrostatic arguments, resulting in a preferential formation of polysulfide species with low charge densities. Therefore, the trends observed from Figure 10 (i.e., increase of both ΔE_D and ΔG_D with decreasing chain length of the bare polysulfide anion) counterbalance the respective trends shown in Figure 9 (decrease of the contact ion pair formation free energy ΔG_{CIP} with decreasing polysulfide

DOI: 10.1021/acs.jpcc.8b06560
J. Phys. Chem. C 2018, 122, 21770–21783

length). The presence of these two antagonistic driving forces suggests that, as a net effect, polysulfide anions with an intermediate charge density are preferentially formed (i.e., S_6^{2-} or S_4^{2-}, depending on the cation species and the solvent).

In order to assess the relative importance of these two opposing trends, we estimate the overall stability of the polysulfide−cation complex from both the values in Figures 9 and 10. To this end, we calculated the change in the contact ion pair formation free energies from Figure 9 (e.g., the difference between Li_2S_8/MgS_8 and Li_2S_6/MgS_6 for the reaction $S_8^{2-} \rightarrow S_6^{2-} + 1/4S_8$), and added this value to the disproportionation free energies from Figure 10 (e.g., $S_8^{2-} \rightarrow S_6^{2-} + 1/4S_8$). The results are shown in Figure 11 as a function of the polysulfide chain length. For the sake of convenience, all energies have been computed relative to the energy values of S_8^{2-}.

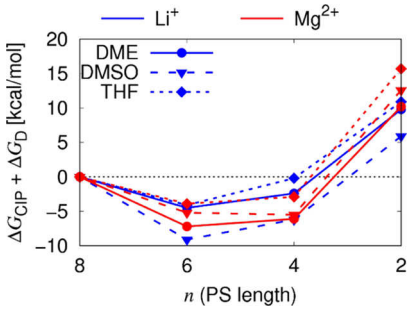

Figure 11. Sum of the change in the contact ion pair formation free energy ΔG_{CIP} (Figure 9) and the disproportionation free energies ΔG_D (Figure 10) for Li and Mg polysulfides in larger cation/polysulfide/solvent clusters as a function of the polysulfide chain length n (in terms of monomers). DMSO, THF, and DME have been used as solvents. The reaction free energies of the bare polysulfides were calculated at the G4MP2 level of theory, the contact ion pair formation free energies were calculated at the PBE/6-31+G(d,p) level of theory including a G4MP2 correction (see text for further details).

From Figure 11, we find that both S_6^{2-} and S_4^{2-} display negative values for the total free energies in all cases, thus rationalizing the disproportionation of the initially present Li_2S_8 and MgS_8 salts to shorter polysulfide salts observed experimentally. Thus, unlike in the CV experiments, where additional reduction processes yield shorter polysulfides, the cation species and its detailed solvation structure is crucial for the formation of those polysulfide species different than S_8^{2-}. When comparing the results for "Li_2S_8" and "MgS_8", we note that S_4^{2-} is more stabilized in the presence of Mg^{2+} than for Li^+. This finding can be rationalized by the enhanced coordination of the bivalent magnesium cations to polysulfide anions with high charge densities (Figure 9), in agreement with the experimental data. Nevertheless, our calculations suggest that the formation of the S_2^{2-} is thermodynamically unfavorable in the presence of both Li^+ and Mg^{2+} despite its strong stabilization by the cation. This is likely because only contact ion pair formation of Li_2S_2 and MgS_2, but no further aggregation was considered in QC calculations. The formation of extended aggregates is expected to stabilize Li_2S_2 and MgS_2 solvates. The latter assumption is verified by calculating the dimerization free energies ΔG_{dimer} for the formal reactions $2Li_2S_2 \rightarrow Li_4(S_2)_2$ and $2MgS_2 \rightarrow Mg_2(S_2)_2$ at the G4MP2 level (without explicit solvent, see also discussion below and Table S4). Here, the Li_2S_2 and MgS_2 appear to have a stronger tendency to form aggregates than the S_4^{2-} or S_6^{2-} species. In particular, we find −29, −23 and −26 kcal/mol for the formation of $Li_4(S_2)_2$ in DME, DMSO, and THF, whereas the respective values for $Mg_2(S_2)_2$ are even larger with ΔG_{dimer} = −54 kcal/mol (DME), −33 kcal/mol (DMSO), −45 kcal/mol (THF). Of course, due to the absence of an explicit solvation shell, these values likely overestimate the true dimerization free energies.

So far, we limited ourselves to bivalent polysulfide species. Experimentally, however, the $S_3^{\bullet-}$ radical anion is another relevant species. Table S2 also shows the contact ion pair formation energies/free energies for $S_3^{\bullet-}$, and Table S3 also lists the dissociation energies and free energies of the reaction $S_6^{2-} \rightarrow 2S_3^{\bullet-}$. The respective dissociation free energies of −3 kcal/mol (DMSO), −10 kcal/mol (THF), and −17 kcal/mol (DME) indicate that from a thermodynamic point of view, free S_6^{2-} should almost completely dissociate into $S_3^{\bullet-}$ (Table S3). On the other hand, however, the comparatively strong stabilization of S_6^{2-} by the cations would render dissociation unfavorable, especially due to the fact that ion pairs involving $S_3^{\bullet-}$ are only stabilized by free energy differences in the range of −13 to −4 kcal/mol for "Li_2S_8", and by −27 kcal/mol (DME) or −21 kcal/mol (THF) for "MgS_8", while no stable ion pairs are predicted in DMSO for the latter cation (Table S2). Thus, the monovalent charge of $S_3^{\bullet-}$ leads to weaker ion pairing for this species. For these reasons, $S_3^{\bullet-}$ might be more loosely solvated, although the UV/vis results clearly indicate that both the employed cation species and solvation effects still play an important role (especially in the ethers).

Such rather subtle solvation changes make also the quantitative characterization of the relative polysulfide populations based on the data presented in Figure 11 a formidable task due to numerous assumptions such as neglect of the large aggregates and consideration of only the contact ion pair formation. Our CCA also could not explicitly take into account salt concentration that was experimentally shown to play an important role in shifting reaction equilibrium, especially for the weakly solvating solvents. Here, especially the difference between S_6^{2-} and S_4^{2-} is on the order of a few kcal/mol only, which is on the order of accuracy of G4MP2 method that has the average error of ≈1 kcal/mol.[49] The presence of a distribution of solvation shell structures—likely to be encountered in thermodynamic equilibrium—therefore biases the delicate balance between these two dianions, in agreement with the experimentally observed coexistence of multiple species. Capturing these effects therefore rather requires a molecular-dynamics approach, either relying on well-parametrized force fields[80] or first principles.[81] Indeed, in the latter publication, it was shown that long lithium polysulfides may also exist as effective $Li^+-LiS_n^-$ ion pairs involving a strongly and a weakly coordinated lithium ion.[81] Moreover, these simulations also revealed a significant entropic stabilization of solvated S_8 molecules (and presumably also for fully solvated polysulfide anions), which is not captured by the implicit SMD solvation model. Neglecting these fine details of the polysulfide and polysulfide complex solvation, our results clearly emphasize the importance of polysulfide stabilization via both, the cation species and the solvent, as well as the resulting impact on the disproportionation reactions.

Apart from slight differences in the coordination sphere, one might also imagine the formation of larger ion clusters, for

DOI: 10.1021/acs.jpcc.8b06560
J. Phys. Chem. C 2018, 122, 21770−21783

which, however, the calculations based on the CCA with explicit solvent molecules rapidly become too costly. In order to estimate the main impact of such a clustering on the distribution of polysulfide species, we performed G4MP2 calculations (i.e., without explicit solvent molecules) for the aggregation of an ion pair to a dimeric cluster, as described by the formal reaction equations $2Li_2S_4 \rightarrow Li_4(S_4)_2$, $2Li_2S_6 \rightarrow Li_4(S_6)_2$, $2MgS_4 \rightarrow Mg_2(S_4)_2$, and $2MgS_6 \rightarrow Mg_2(S_6)_2$. The results for the dimerization free energies ΔG_{dimer} are shown in Table S4. Although the resulting free energies likely predict too strong clustering of ion pairs due to the lack of an explicit solvation shell, we note that clustering is expected to be more pronounced for the magnesium salts. In particular, for both Li_2S_4 and Li_2S_6, we find comparable dimerization free energies in the range of −9 to −4 kcal/mol in all solvents, whereas MgS_4 shows a substantially larger tendency to aggregate in the ethers than MgS_6 (ΔG_{dimer} = −22 kcal/mol vs ΔG_{dimer} = −8 kcal/mol in DME, and ΔG_{dimer} = −16 kcal/mol vs ΔG_{dimer} = −9 kcal/mol in THF). Conversely, in DMSO, only the aggregation of MgS_4 appears to be thermodynamically stable. Therefore, these results suggest that the formation of larger ion clusters shifts the polysulfide equilibrium towards S_4^{2-}, as observed experimentally.

Due to the delicate balance between cation stabilization and disproportionation, the polysulfide equilibrium can be rather easily shifted by other electrolyte components (especially salts), such as LiTFSI/$MgTFSI_2$ in the present case (see above). For these reasons, we also computed the contact ion pair formation energies for solvated LiTFSI and $MgTFSI^+$ clusters (Table S2). (Here, we restricted ourselves to the bidentate TFSI coordination.[46]) For LiTFSI, ΔG_{CIP} is in the range of −9 to −4 kcal/mol in the ether solvents THF and DME, and ≈−3 kcal/mol in DMSO. Such an aggregation behavior is consistent with the experimentally measured ionicity values for LiTFSI[82] and results of MD simulations for DME−LiTFSI.[83] For $MgTFSI^+$, we find values of −23 kcal/mol (DME) and −24 kcal/mol (THF) for the ethers, while in DMSO the complex is unstable, as indicated by a positive value of ΔG_{CIP} = 5 kcal/mol. In total, when comparing these numbers with the respective values for the bivalent polysulfide anions (Table S2), it is evident that the interaction of the cations with TFSI is significantly smaller than for the polysulfides. Therefore, the addition of TFSI salts does not lead to the release of free polysulfide anions due to competing interactions of TFSI and the polysulfides for the cations themselves. Nevertheless, in the ethers, ΔG_{CIP} is negative, such that LiTFSI and $Mg(TFSI)_2$ aggregates are likely to form, which in principle may also participate in larger $MgS_n(TFSI)_m$ and (to a smaller extend) $Li_2S_n(TFSI)_m$ clusters. Furthermore, due to the increased overall ion concentration, larger ionic aggregates are more likely to form, which would also substantially affect the stability of the individual polysulfide species. This is also due to the fact that in the abundance of cations, both TFSI and the polysulfide chains may coordinate to two cations simultaneously, bridging them in this way. Such an ion clustering would lead to more complicated reduction/oxidation processes and solvation/desolvation mechanisms, while at the same time provide additional control parameters for shifting redox reactions towards specific potentials, and to tune the polysulfide solubility. It is questionable in how far these results can be generalized to salts with other anions. However, in case of chloride anions, it is known that Mg^{2+} forms cationic $Mg_xCl_y^+$ species,[84] which might also influence the redox processes and solubility of Mg polysulfides.

CONCLUSIONS

In this study we demonstrated that the reduction and oxidation processes, thus mechanisms, of Li and Mg polysulfide solutions differ substantially. In the high-ε solvents DMSO, DMF, and ACN, these differences are generally related to a poorer stabilization of low charge density ("long-chain") polysulfides S_8^{2-}, S_6^{2-} and especially $S_3^{\bullet-}$ in presence of Mg^{2+} instead of Li^+. Whereas in DMSO and DMF, only the polysulfide oxidation mechanism is affected by these differences, they also determine the reduction pathway in ACN. In the low-ε solvents DME and TEGDME, the reduction of sulfur proceeds via S_4^{2-} to S_2^{2-}, when Li^+ cations are present. In contrast, in case of coordination by Mg^{2+}, only the direct reduction of sulfur to S_2^{2-} is observed. A similar behavior is shown in the Li and Mg polysulfide solutions in THF. In addition, the oxidation of Mg polysulfides in DME, TEGDME, THF, and ACN solutions was observed to occur at substantially higher potentials than in their Li counterparts.

QC calculations indicate that ion pairing in Mg polysulfide solutions is more pronounced than in their Li counterparts. As short and highly charged polysulfides, like S_4^{2-} and S_2^{2-}, are generally more stabilized by cation coordination, the calculations explain why the disproportionation in the Mg polysulfides in ethers is more pronounced than that of Li polysulfides of the respective solutions. In addition, preliminary results confirm that the dissociation of S_6^{2-} to $S_3^{\bullet-}$ is less favored in case of Mg^{2+} coordination.

In conclusion, this study sheds light on the different discharge/charge mechanisms of the sulfur cathode in Li/S and Mg/S batteries. Thereby, it gives an additional explanation for the high overvoltages of current Mg/S cells. The comparison of the apparently poor Mg polysulfide electrochemistry in currently used ethers with the better performance in solvents like DMSO and DMF emphasizes the importance of the electrolyte solvent. Lowering the overpotentials of the sulfur cathode in Mg/S batteries is a fundamental challenge for achieving reasonable energy density and efficiency. This challenge might be overcome by the use of ionic liquids. In ongoing research, we found low overpotentials of sulfur formation in both, Li and Mg polysulfide solutions in $Pyr_{14}TFSI$. In addition, ionic liquids are considered to suppress polysulfide dissolution in Li/S[85−88] and Mg/S[26,27] batteries.

Besides clarifying the influence of the solvent, this study gives an insight in the role of the cation in determining the charge and discharge mechanism of the sulfur cathode. It is demonstrated that the electrochemistry of the sulfur cathode differs fundamentally with coordination by the monovalent Li^+ or the bivalent Mg^{2+}. Accordingly, Gao et al. observed that the re-oxidation of MgS and MgS_2 and thus the reversibility of Mg/S cells is substantially improved by the addition of LiTFSI.[30] Such hybrid Li/Mg electrolytes might thus also path the way to more efficient Mg/S batteries.

Furthermore, a deeper understanding of the cation coordination by the solvent and its interaction with the polysulfide species might also improve the electrolytes of Li/S batteries and support the development of other multivalent metal/sulfur battery systems.

DOI: 10.1021/acs.jpcc.8b06560
J. Phys. Chem. C 2018, 122, 21770−21783

■ ASSOCIATED CONTENT

Supporting Information

The Supporting Information is available free of charge on the ACS Publications website at DOI: 10.1021/acs.jpcc.8b06560.

Supplementary data including further UV/vis spectra, the CV cell set-up and additional cyclic voltammograms, as well as the tables and geometries of the contact ion pair clusters corresponding to the QC calculations (PDF)

■ AUTHOR INFORMATION

Corresponding Authors

*E-mail: martin.kolek@uni-muenster.de. Phone: +49 251 83-36024.

*E-mail: peter.bieker@uni-muenster.de. Phone: +49 251 83-36750.

ORCID

Diddo Diddens: 0000-0002-2137-1332

Martin Kolek: 0000-0001-7852-4064

Oleg Borodin: 0000-0002-9428-5291

Peter Bieker: 0000-0003-4378-4805

Present Address

[‖]Akkurate Oy, Kaarikatu 8b, 20760 Kaarina, Finland.

Author Contributions

All authors have given approval to the final version of the manuscript.

Notes

The authors declare no competing financial interest.

■ ACKNOWLEDGMENTS

The authors wish to thank the German Ministry of Education and Research (BMBF) for funding of this work through the projects "MgMeAnS" (03XP0140) and "ACHiLiS" (03XP0037A). They further thank the Heinrich Böll Foundation for the funding through a PhD scholarship.

■ REFERENCES

(1) Wagner, R.; Preschitschek, N.; Passerini, S.; Leker, J.; Winter, M. Current Research Trends and Prospects among the Various Materials and Designs Used in Lithium-Based Batteries. *J. Appl. Electrochem.* **2013**, *43*, 481−496.

(2) Placke, T.; Kloepsch, R.; Dühnen, S.; Winter, M. Lithium Ion, Lithium Metal, and Alternative Rechargeable Battery Technologies: The Odyssey for High Energy Density. *J. Solid State Electrochem.* **2017**, *21*, 1939−1964.

(3) Nazar, L. F.; Cuisinier, M.; Pang, Q. Lithium-Sulfur Batteries. *MRS Bull.* **2014**, *39*, 436−442.

(4) Manthiram, A.; Fu, Y.; Chung, S.-H.; Zu, C.; Su, Y.-S. Rechargeable Lithium-Sulfur Batteries. *Chem. Rev.* **2014**, *114*, 11751−11787.

(5) Schmuch, R.; Wagner, R.; Hörpel, G.; Placke, T.; Winter, M. Performance and Cost of Materials for Lithium-Based Rechargeable Automotive Batteries. *Nat. Energy* **2018**, *3*, 267−278.

(6) Winter, M. The Solid Electrolyte Interphase - The Most Important and the Least Understood Solid Electrolyte in Rechargeable Li Batteries. *Z. Phys. Chem.* **2009**, *223*, 1395−1406.

(7) Peled, E.; Golodnitsky, D.; Ardel, G. Advanced Model for Solid Electrolyte Interphase Electrodes in Liquid and Polymer Electrolytes. *J. Electrochem. Soc.* **1997**, *144*, L208−L210.

(8) Aurbach, D.; Zinigrad, E.; Cohen, Y.; Teller, H. A Short Review of Failure Mechanisms of Lithium Metal and Lithiated Graphite Anodes in Liquid Electrolyte Solutions. *Solid State Ionics* **2002**, *148*, 405−416.

(9) Bieker, G.; Winter, M.; Bieker, P. Electrochemical in Situ Investigations of SEI and Dendrite Formation on the Lithium Metal Anode. *Phys. Chem. Chem. Phys.* **2015**, *17*, 8670−8679.

(10) Becking, J.; Gröbmeyer, A.; Kolek, M.; Rodehorst, U.; Schulze, S.; Winter, M.; Bieker, P.; Stan, M. C. Lithium-Metal Foil Surface Modification: An Effective Method to Improve the Cycling Performance of Lithium-Metal Batteries. *Adv. Mater. Interfaces* **2017**, *4*, 1700166.

(11) Heine, J.; Hilbig, P.; Qi, X.; Niehoff, P.; Winter, M.; Bieker, P. Fluoroethylene Carbonate as Electrolyte Additive in Tetraethylene Glycol Dimethyl Ether Based Electrolytes for Application in Lithium Ion and Lithium Metal Batteries. *J. Electrochem. Soc.* **2015**, *162*, A1094−A1101.

(12) Kanamura, K.; Tamura, H.; Shiraishi, S.; Takehara, Z.-i. Morphology and Chemical Compositions of Surface Films of Lithium Deposited on a Ni Substrate in Nonaqueous Electrolytes. *J. Electroanal. Chem.* **1995**, *394*, 49−62.

(13) Brissot, C.; Rosso, M.; Chazalviel, J.-N.; Lascaud, S. Dendritic Growth Mechanisms in Lithium/Polymer Cells. *J. Power Sources* **1999**, *81*−*82*, 925−929.

(14) Cohen, Y. S.; Cohen, Y.; Aurbach, D. Micromorphological Studies of Lithium Electrodes in Alkyl Carbonate Solutions Using in Situ Atomic Force Microscopy. *J. Phys. Chem. B* **2000**, *104*, 12282−12291.

(15) Ryou, M.-H.; Lee, Y. M.; Lee, Y.; Winter, M.; Bieker, P. Mechanical Surface Modification of Lithium Metal: Towards Improved Li Metal Anode Performance by Directed Li Plating. *Adv. Funct. Mater.* **2015**, *25*, 834−841.

(16) Wedepohl, K. H. The Composition of the Continental Crust. *Geochim. Cosmochim. Acta* **1995**, *59*, 1217−1232.

(17) Angino, E. E.; Billings, G. K. Lithium Content of Sea Water by Atomic Absorption Spectrometry. *Geochim. Cosmochim. Acta* **1966**, *30*, 153−158.

(18) Riley, J. P.; Tongudai, M. The Lithium Content of Sea Water. *Deep-Sea Res. Oceanogr. Abstr.* **1964**, *11*, 563−568.

(19) Meister, P.; Jia, H.; Li, J.; Kloepsch, R.; Winter, M.; Placke, T. Best Practice: Performance and Cost Evaluation of Lithium Ion Battery Active Materials with Special Emphasis on Energy Efficiency. *Chem. Mater.* **2016**, *28*, 7203−7217.

(20) Gao, T.; Li, X.; Wang, X.; Hu, J.; Han, F.; Fan, X.; Suo, L.; Pearse, A. J.; Lee, S. B.; Rubloff, G. W.; et al. A Rechargeable Al/S Battery with an Ionic-Liquid Electrolyte. *Angew. Chem.* **2016**, *128*, 10052−10055.

(21) Yang, H.; Yin, L.; Liang, J.; Sun, Z.; Wang, Y.; Li, H.; He, K.; Ma, L.; Peng, Z.; Qiu, S.; et al. An Aluminum−Sulfur Battery with a Fast Kinetic Response. *Angew. Chem., Int. Ed.* **2018**, *57*, 1898.

(22) Ponrouch, A.; Frontera, C.; Bardé, F.; Palacín, M. R. Towards a Calcium-Based Rechargeable Battery. *Nat. Mater.* **2016**, *15*, 169−172.

(23) Wang, D.; Gao, X.; Chen, Y.; Jin, L.; Kuss, C.; Bruce, P. G. Plating and Stripping Calcium in an Organic Electrolyte. *Nat. Mater.* **2017**, *17*, 16−20.

(24) Kim, H. S.; Arthur, T. S.; Allred, G. D.; Zajicek, J.; Newman, J. G.; Rodnyansky, A. E.; Oliver, A. G.; Boggess, W. C.; Muldoon, J. Structure and Compatibility of a Magnesium Electrolyte with a Sulphur Cathode. *Nat. Commun.* **2011**, *2*, 427.

(25) Ha, S.-Y.; Lee, Y.-W.; Woo, S. W.; Koo, B.; Kim, J.-S.; Cho, J.; Lee, K. T.; Choi, N.-S. Magnesium(II) Bis(Trifluoromethane Sulfonyl) Imide-Based Electrolytes with Wide Electrochemical Windows for Rechargeable Magnesium Batteries. *ACS Appl. Mater. Interfaces* **2014**, *6*, 4063−4073.

(26) Zhao-Karger, Z.; Zhao, X.; Wang, D.; Diemant, T.; Behm, R. J.; Fichtner, M. Performance Improvement of Magnesium Sulfur Batteries with Modified Non-Nucleophilic Electrolytes. *Adv. Energy Mater.* **2015**, *5*, 1401155.

(27) Li, W.; Cheng, S.; Wang, J.; Qiu, Y.; Zheng, Z.; Lin, H.; Nanda, S.; Ma, Q.; Xu, Y.; Ye, F.; et al. Synthesis, Crystal Structure, and Electrochemical Properties of a Simple Magnesium Electrolyte

DOI: 10.1021/acs.jpcc.8b06560
J. Phys. Chem. C 2018, 122, 21770−21783

for Magnesium/Sulfur Batteries. *Angew. Chem.* **2016**, *128*, 6516−6520.
(28) Zhang, Z.; Cui, Z.; Qiao, L.; Guan, J.; Xu, H.; Wang, X.; Hu, P.; Du, H.; Li, S.; Zhou, X.; et al. Novel Design Concepts of Efficient Mg-Ion Electrolytes toward High-Performance Magnesium-Selenium and Magnesium-Sulfur Batteries. *Adv. Energy Mater.* **2017**, *7*, 1602055.
(29) Gao, T.; Hou, S.; Wang, F.; Ma, Z.; Li, X.; Xu, K.; Wang, C. Reversible S0 /MgS x Redox Chemistry in a MgTFSI2 /MgCl2 /DME Electrolyte for Rechargeable Mg/S Batteries. *Angew. Chem.* **2017**, *129*, 13711−13715.
(30) Gao, T.; Noked, M.; Pearse, A. J.; Gillette, E.; Fan, X.; Zhu, Y.; Luo, C.; Suo, L.; Schroeder, M. A.; Xu, K.; et al. Enhancing the Reversibility of Mg/S Battery Chemistry through Li+ Mediation. *J. Am. Chem. Soc.* **2015**, *137*, 12388−12393.
(31) Vinayan, B. P.; Zhao-Karger, Z.; Diemant, T.; Chakravadhanula, V. S. K.; Schwarzburger, N. I.; Cambaz, M. A.; Behm, R. J.; Kübel, C.; Fichtner, M. Performance Study of Magnesium-Sulfur Battery Using a Graphene Based Sulfur Composite Cathode Electrode and a Non-Nucleophilic Mg Electrolyte. *Nanoscale* **2016**, *8*, 3296−3306.
(32) Yu, X.; Manthiram, A. Performance Enhancement and Mechanistic Studies of Magnesium-Sulfur Cells with an Advanced Cathode Structure. *ACS Energy Lett.* **2016**, *1*, 431−437.
(33) Zhao-Karger, Z.; Gil Bardaji, M. E.; Fuhr, O.; Fichtner, M. A New Class of Non-Corrosive, Highly Efficient Electrolytes for Rechargeable Magnesium Batteries. *J. Mater. Chem. A* **2017**, *5*, 10815−10820.
(34) Sievert, B.; Häcker, J.; Bienen, F.; Wagner, N.; Friedrich, K. A. Magnesium Sulfur Battery with a New Magnesium Powder Anode. *ECS Trans.* **2017**, *77*, 413−424.
(35) Robba, A.; Vizintin, A.; Bitenc, J.; Mali, G.; Arčon, I.; Kavčič, M.; Žitnik, M.; Bučar, K.; Aquilanti, G.; Martineau-Corcos, C.; et al. Mechanistic Study of Magnesium-Sulfur Batteries. *Chem. Mater.* **2017**, *29*, 9555−9564.
(36) Gao, T.; Ji, X.; Hou, S.; Fan, X.; Li, X.; Yang, C.; Han, F.; Wang, F.; Jiang, J.; Xu, K.; et al. Thermodynamics and Kinetics of Sulfur Cathode during Discharge in MgTFSI2 -DME Electrolyte. *Adv. Mater.* **2018**, *30*, 1704313.
(37) Shterenberg, I.; Salama, M.; Yoo, H. D.; Gofer, Y.; Park, J.-B.; Sun, Y.-K.; Aurbach, D. Evaluation of (CF3SO2)2N−(TFSI) Based Electrolyte Solutions for Mg Batteries. *J. Electrochem. Soc.* **2015**, *162*, A7118−A7128.
(38) Doe, R. E.; Han, R.; Hwang, J.; Gmitter, A. J.; Shterenberg, I.; Yoo, H. D.; Pour, N.; Aurbach, D. Novel, Electrolyte Solutions Comprising Fully Inorganic Salts with High Anodic Stability for Rechargeable Magnesium Batteries. *Chem. Commun.* **2014**, *50*, 243−245.
(39) Zhao-Karger, Z.; Zhao, X.; Fuhr, O.; Fichtner, M. Bisamide Based Non-Nucleophilic Electrolytes for Rechargeable Magnesium Batteries. *RSC Adv.* **2013**, *3*, 16330−16335.
(40) Zu, C.-X.; Li, H. Thermodynamic Analysis on Energy Densities of Batteries. *Energy Environ. Sci.* **2011**, *4*, 2614−2624.
(41) U.S. Geological Survey. *Mineral Commodity Summaries 2018*; USGS, 2018.
(42) Millero, F. J.; Feistel, R.; Wright, D. G.; McDougall, T. J. The Composition of Standard Seawater and the Definition of the Reference-Composition Salinity Scale. *Deep Sea Res., Part I* **2008**, *55*, 50−72.
(43) Bieker, G.; Wellmann, J.; Kolek, M.; Jalkanen, K.; Winter, M.; Bieker, P. Influence of Cations in Lithium and Magnesium Polysulphide Solutions: Dependence of the Solvent Chemistry. *Phys. Chem. Chem. Phys.* **2017**, *19*, 11152−11162.
(44) Dev, S.; Ramli, E.; Rauchfuss, T. B.; Wilson, S. R. Synthesis and structure of [M(N-methylimidazole)6]S8 (M = manganese, iron, nickel, magnesium). Polysulfide salts prepared by the reaction N-methylimidazole + metal powder + sulfur. *Inorg. Chem.* **1991**, *30*, 2514−2519.
(45) Frisch, M.; Trucks, G.; Schlegel, H. B.; Scuseria, G. E.; Robb, M. A.; Cheeseman, J. R.; Scalmani, G.; Barone, V.; Mennucci, B.; Petersson, G. *Gaussian 09*, Revision A.2; Gaussian. Inc.: Wallingford, CT, 2009.
(46) Chapman, N.; Borodin, O.; Yoon, T.; Nguyen, C. C.; Lucht, B. L. Spectroscopic and Density Functional Theory Characterization of Common Lithium Salt Solvates in Carbonate Electrolytes for Lithium Batteries. *J. Phys. Chem. C* **2017**, *121*, 2135−2148.
(47) Borodin, O.; Olguin, M.; Ganesh, P.; Kent, P. R. C.; Allen, J. L.; Henderson, W. A. Competitive Lithium Solvation of Linear and Cyclic Carbonates from Quantum Chemistry. *Phys. Chem. Chem. Phys.* **2016**, *18*, 164−175.
(48) Perdew, J. P.; Burke, K.; Ernzerhof, M. Generalized Gradient Approximation Made Simple. *Phys. Rev. Lett.* **1996**, *77*, 3865−3868.
(49) Curtiss, L. A.; Redfern, P. C.; Raghavachari, K. Gaussian-4 Theory Using Reduced Order Perturbation Theory. *J. Chem. Phys.* **2007**, *127*, 124105.
(50) Grimme, S.; Ehrlich, S.; Goerigk, L. Effect of the Damping Function in Dispersion Corrected Density Functional Theory. *J. Comput. Chem.* **2011**, *32*, 1456−1465.
(51) Boys, S. F.; Bernardi, F. The Calculation of Small Molecular Interactions by the Differences of Separate Total Energies. Some Procedures with Reduced Errors. *Mol. Phys.* **1970**, *19*, 553−566.
(52) Marenich, A. V.; Cramer, C. J.; Truhlar, D. G. Universal Solvation Model Based on Solute Electron Density and on a Continuum Model of the Solvent Defined by the Bulk Dielectric Constant and Atomic Surface Tensions. *J. Phys. Chem. B* **2009**, *113*, 6378−6396.
(53) Reinsberg, P.; Bondue, C.; Baltruschat, H. Mechanistic Investigation of the Oxygen Reduction in Magnesium Ion-Containing Dimethyl Sulfoxide. *Electrochim. Acta* **2016**, *200*, 214−221.
(54) Fischer, P.; Schwarz, R. M.; Marinaro, M.; Wachtler, M.; Jörissen, L. Investigation of the Electrochemical Oxygen Reduction Reaction in Non-Aqueous, Magnesium-Ion-Containing Electrolytes for Magnesium Air Batteries. *ECS Trans.* **2017**, *75*, 3−12.
(55) Maeda, Y.; Touzain, P. Metal Ion Intercalation on Graphite Cathode in $MgCl_2$ DMSO and $MnCl_2$ DMSO Solutions. *Electrochim. Acta* **1988**, *33*, 1493−1497.
(56) Shiga, T.; Hase, Y.; Kato, Y.; Inoue, M.; Takechi, K. A rechargeable non-aqueous Mg-O2 battery. *Chem. Commun.* **2013**, *49*, 9152−9154.
(57) Gregory, T. D.; Hoffman, R. J.; Winterton, R. C. Nonaqueous Electrochemistry of Magnesium. *J. Electrochem. Soc.* **1990**, *137*, 775−780.
(58) God, C.; Bitschnau, B.; Kapper, K.; Lenardt, C.; Schmuck, M.; Mautner, F.; Koller, S. Intercalation Behaviour of Magnesium into Natural Graphite Using Organic Electrolyte Systems. *RSC Adv.* **2017**, *7*, 14168−14175.
(59) Tran, T. T.; Lamanna, W. M.; Obrovac, M. N. Evaluation of Mg[N(SO2CF3)2]2/Acetonitrile Electrolyte for Use in Mg-Ion Cells. *J. Electrochem. Soc.* **2012**, *159*, A2005−A2009.
(60) Zeng, J.; Yang, Y.; Li, C.; Li, J.; Huang, J.; Wang, J.; Zhao, J. Li3VO4: an insertion anode material for magnesium ion batteries with high specific capacity. *Electrochim. Acta* **2017**, *247*, 265−270.
(61) Arthur, T. S.; Singh, N.; Matsui, M. Electrodeposited Bi, Sb and Bi1-xSbx alloys as anodes for Mg-ion batteries. *Electrochem. Commun.* **2012**, *16*, 103−106.
(62) Lu, Y.-C.; He, Q.; Gasteiger, H. A. Probing the Lithium-Sulfur Redox Reactions: A Rotating-Ring Disk Electrode Study. *J. Phys. Chem. C* **2014**, *118*, 5733−5741.
(63) Zou, Q.; Lu, Y.-C. Solvent-Dictated Lithium Sulfur Redox Reactions: An Operando UV-vis Spectroscopic Study. *J. Phys. Chem. Lett.* **2016**, *7*, 1518−1525.
(64) Kim, B.-S.; Park, S. M. In Situ Spectroelectrochemical Studies on the Reduction of Sulfur in Dimethyl Sulfoxide Solutions. *J. Electrochem. Soc.* **1993**, *140*, 115−122.

DOI: 10.1021/acs.jpcc.8b06560
J. Phys. Chem. C 2018, 122, 21770−21783

(65) Martin, R. P.; Doub, W. H.; Roberts, J. L.; Sawyer, D. T. Electrochemical Reduction of Sulfur in Aprotic Solvents. *Inorg. Chem.* **1973**, *12*, 1921−1925.
(66) Jung, Y. K.; Kim, S.; Kim, B.-S.; Han, D.-H.; Park, S.-M.; Kwak, J. Effect of Organic Solvents and Electrode Materials on Electrochemical Reduction of Sulfur. *Int. J. Electrochem. Sci.* **2008**, *3*, 566−577.
(67) Han, D.-H.; Kim, B.-S.; Choi, S.-J.; Jung, Y.; Kwak, J.; Park, S.-M. Time-Resolved In Situ Spectroelectrochemical Study on Reduction of Sulfur in N,N′-Dimethylformamide. *J. Electrochem. Soc.* **2004**, *151*, E283−E290.
(68) Gaillard, F.; Levillain, E. Visible time-resolved spectroelectrochemistry: application to study of the reduction of sulfur (S8) in dimethylformamide. *J. Electroanal. Chem.* **1995**, *398*, 77−87.
(69) Evans, A.; Montenegro, M. I.; Pletcher, D. The Mechanism for the Cathodic Reduction of Sulphur in Dimethylformamide: Low Temperature Voltammetry. *Electrochem. Commun.* **2001**, *3*, 514−518.
(70) Tutusaus, O.; Mohtadi, R. Paving the Way Towards Highly Stable and Practical Electrolytes for Rechargeable Magnesium Batteries. *ChemElectroChem* **2015**, *2*, 51−57.
(71) Lossius, L. P.; Emmenegger, F. Plating of Magnesium from Organic Solvents. *Electrochim. Acta* **1996**, *41*, 445−447.
(72) Son, S.-B.; Gao, T.; Harvey, S. P.; Steirer, K. X.; Stokes, A.; Norman, A.; Wang, C.; Cresce, A.; Xu, K.; Ban, C. An Artificial Interphase Enables Reversible Magnesium Chemistry in Carbonate Electrolytes. *Nat. Chem.* **2018**, *10*, 532−539.
(73) Yan, Y.; Khoo, T.; Pozo-Gonzalo, C.; Hollenkamp, A. F.; Howlett, P. C.; MacFarlane, D. R.; Forsyth, M. Roles of Additives in the Trihexyl(Tetradecyl) Phosphonium Chloride Ionic Liquid Electrolyte for Primary Mg-Air Cells. *J. Electrochem. Soc.* **2014**, *161*, A974−A980.
(74) Fujinaga, T.; Kuwamoto, T.; Okazaki, S.; Hojo, M. Electrochemical Reduction of Elemental Sulfur in Acetonitrile. *Bull. Chem. Soc. Jpn.* **1980**, *53*, 2851−2855.
(75) Gutmann, V. Solvent Effects on the Reactivities of Organometallic Compounds. *Coord. Chem. Rev.* **1976**, *18*, 225−255.
(76) Barchasz, C.; Molton, F.; Duboc, C.; Leprêtre, J.-C.; Patoux, S.; Alloin, F. Lithium/Sulfur Cell Discharge Mechanism: An Original Approach for Intermediate Species Identification. *Anal. Chem.* **2012**, *84*, 3973−3980.
(77) Marceau, H.; Kim, C.-S.; Paolella, A.; Ladouceur, S.; Lagacé, M.; Chaker, M.; Vijh, A.; Guerfi, A.; Julien, C. M.; Mauger, A.; et al. In Operando Scanning Electron Microscopy and Ultraviolet-Visible Spectroscopy Studies of Lithium/Sulfur Cells Using All-Solid-State Polymer Electrolyte. *J. Power Sources* **2016**, *319*, 247−254.
(78) Curtiss, L. A.; Redfern, P. C.; Raghavachari, K. Gn Theory. *Wiley Interdiscip. Rev.: Comput. Mol. Sci.* **2011**, *1*, 810−825.
(79) Assary, R. S.; Curtiss, L. A.; Moore, J. S. Toward a Molecular Understanding of Energetics in Li-S Batteries Using Nonaqueous Electrolytes: A High-Level Quantum Chemical Study. *J. Phys. Chem. C* **2014**, *118*, 11545−11558.
(80) Yang, C.; Suo, L.; Borodin, O.; Wang, F.; Sun, W.; Gao, T.; Fan, X.; Hou, S.; Ma, Z.; Amine, K.; et al. Unique Aqueous Li-Ion/Sulfur Chemistry with High Energy Density and Reversibility. *Proc. Natl. Acad. Sci. U.S.A.* **2017**, *114*, 6197−6202.
(81) Pascal, T. A.; Wujcik, K. H.; Wang, D. R.; Balsara, N. P.; Prendergast, D. Thermodynamic Origins of the Solvent-Dependent Stability of Lithium Polysulfides from First Principles. *Phys. Chem. Chem. Phys.* **2017**, *19*, 1441−1448.
(82) Hayamizu, K.; Aihara, Y.; Arai, S.; Martinez, C. G. Pulse-Gradient Spin-Echo ^{1}H, ^{7}Li, and ^{19}F NMR Diffusion and Ionic Conductivity Measurements of 14 Organic Electrolytes Containing $LiN(SO_2CF_3)_2$. *J. Phys. Chem. B* **1999**, *103*, 519−524.
(83) Borodin, O.; Smith, G. D. Development of Many−Body Polarizable Force Fields for Li-Battery Applications: 2. LiTFSI-Doped Oligoether, Polyether, and Carbonate-Based Electrolytes. *J. Phys. Chem. B* **2006**, *110*, 6293−6299.
(84) Salama, M.; Shterenberg, I.; Shimon, L. J. W.; Keinan-Adamsky, M.; Gofer, Y.; Aurbach, D. Structural Analysis of Magnesium Chloride Complexes in Dimethoxyethane Solutions in the Context of Mg Batteries Research. *J. Phys. Chem. C* **2017**, *121*, 24909−24918.
(85) Wang, J.; Chew, S. Y.; Zhao, Z. W.; Ashraf, S.; Wexler, D.; Chen, J.; Ng, S. H.; Chou, S. L.; Liu, H. K. Sulfur-Mesoporous Carbon Composites in Conjunction with a Novel Ionic Liquid Electrolyte for Lithium Rechargeable Batteries. *Carbon* **2008**, *46*, 229−235.
(86) Park, J.-W.; Ueno, K.; Tachikawa, N.; Dokko, K.; Watanabe, M. Ionic Liquid Electrolytes for Lithium-Sulfur Batteries. *J. Phys. Chem. C* **2013**, *117*, 20531−20541.
(87) Park, J.-W.; Yamauchi, K.; Takashima, E.; Tachikawa, N.; Ueno, K.; Dokko, K.; Watanabe, M. Solvent Effect of Room Temperature Ionic Liquids on Electrochemical Reactions in Lithium-Sulfur Batteries. *J. Phys. Chem. C* **2013**, *117*, 4431−4440.
(88) Yuan, L. X.; Feng, J. K.; Ai, X. P.; Cao, Y. L.; Chen, S. L.; Yang, H. X. Improved Dischargeability and Reversibility of Sulfur Cathode in a Novel Ionic Liquid Electrolyte. *Electrochem. Commun.* **2006**, *8*, 610−614.

DOI: 10.1021/acs.jpcc.8b06560
J. Phys. Chem. C 2018, 122, 21770−21783